

Journal of Physics: Complexity

OPEN ACCESS**PAPER**

RECEIVED
16 July 2021

REVISED
9 October 2021

ACCEPTED FOR PUBLICATION
2 November 2021

PUBLISHED
23 November 2021

Original content from
this work may be used
under the terms of the
[Creative Commons
Attribution 4.0 licence](#).

Any further distribution
of this work must
maintain attribution to
the author(s) and the
title of the work, journal
citation and DOI.



First passage dynamics of stochastic motion in heterogeneous media driven by correlated white Gaussian and coloured non-Gaussian noises

Nicholas Mwiliu Mutohya^{1,2}, Yong Xu^{1,*}, Yongge Li¹, Ralf Metzler^{3,*} and Nicholas Muthama Mutua²

¹ School of Mathematics and Statistics, Northwestern Polytechnical University, Xi'an, 710072, People's Republic of China

² Department of Mathematics, Statistics and Physical Sciences, Taifa Taveta University, PO Box 635-80300 Voi, Kenya

³ University of Potsdam, Institute of Physics & Astronomy, 14476 Potsdam, Germany

* Authors to whom any correspondence should be addressed.

E-mail: rmetzler@uni-potsdam.de

Keywords: first passage, diffusion, non-Gaussian, correlated noise

Abstract

We study the first passage dynamics for a diffusing particle experiencing a spatially varying diffusion coefficient while driven by correlated additive Gaussian white noise and multiplicative coloured non-Gaussian noise. We consider three functional forms for position dependence of the diffusion coefficient: power-law, exponential, and logarithmic. The coloured non-Gaussian noise is distributed according to Tsallis' q -distribution. Tracks of the non-Markovian systems are numerically simulated by using the fourth-order Runge–Kutta algorithm and the first passage times (FPTs) are recorded. The FPT density is determined along with the mean FPT (MFPT). Effects of the noise intensity and self-correlation of the multiplicative noise, the intensity of the additive noise, the cross-correlation strength, and the non-extensivity parameter on the MFPT are discussed.

1. Introduction

Modern microscopic techniques allow experimentalists to monitor the active or diffusive motion of small tracers such as virus particles or proteins in the highly heterogeneous environment of living biological cells [1–6]. Concurrently fluorescence experiments show pronounced localisation of specific signalling proteins depending on the position of their encoding gene [7]. Together with findings on the spatial distance in bacterial genomes of a specific gene, controlled by a signalling protein, from the gene encoding this regulator [8, 9] led to the development of new concepts such as geometry control of biochemical reactions in the small concentration limit typical for many processes in intracellular gene expression [8–12]. Such studies represent generalisations of the classical description of molecular chemical reactions at macroscopic concentration levels based on mean reaction rates [13, 14].

A crucial step in molecular reactions is the diffusion limitation, i.e., the time it takes a molecule to reach a reaction centre for the first time after its release a given distance away [13]. This first passage time (FPT) [15, 16] is a general concept finding applications not only in molecular reactions but also in polymer translocation [17], the quantification of the search for food by animals [18] or in the spreading of new diseases such as SARS or Covid [19, 20]. FPT theory is often used to estimate the escape time from a metastable state, trap or potential well, or barrier crossing and phase transition rates [21, 22]. In the geosciences the concept of first passage is at the heart of particle transport in underground aquifers [23] while in finance the first passage to a given stock value determines actions such as buying or selling [24]. The FPT is used to quantify the efficiency of transport and search as well as identify optimal search and transport strategies [25] or to characterise stochastic motion in a heterogeneous environment [26]. The FPT provides information on spatial properties of complex networks [27] or extreme values of random processes [28] and characteristic observables in non-equilibrium systems [29]. The FPT provides information complementary to the mean squared displacement in exploring

the dynamical behaviour of a stochastic motion [30]. Furthermore, it reveals whether a system is following normal or anomalous diffusion and helps to distinguish different anomalous diffusion mechanisms [31, 32]. Finally we mention recent studies on the effect of multiple searchers and their initial distribution in space on the FPT dynamics [33–37]. The statistic of a given FPT process can be explored in terms of the full distribution of FPTs, the FPT density (FTPД) as well as the associated moments, the mean FPT (MFPT) and global MFPT [10, 12, 15, 38]. In different contexts the FPT problem has been investigated theoretically, experimentally as well as by simulations [39–47].

While most theories for FPT dynamics are based on homogeneous descriptions, in many cases one cannot neglect the heterogeneity of the environment. Heterogeneities are inherent in the cytoplasm of biological cells and membranes [2, 32, 48–52] or in granular media [53] and aquifers [23]. They may also be intrinsic in disordered systems such as amorphous semiconductors [54] or complex liquids [55]. Here we are interested in the effects of heterogeneity on the FPT dynamics in such systems. Several recent studies were devoted to generalising stochastic motion in spatially heterogeneous environments, see, e.g. [56, 57]. The dynamical behaviour of heterogeneous diffusion has been explored using the behaviour of the ensemble and time-averaged mean squared displacements. Features such as anomalous diffusion, ergodicity breaking, ageing, and non-Gaussianity have been reported in heterogeneous media [16], see also below.

On top of heterogeneity effects we here also study the resulting FPT dynamics with respect to the noise driving the stochastic motion. This generalisation of the noise includes both the assumption of non-white noise–noise correlations and the relaxation of the Gaussian statistic of the noise amplitude. Multiplicative noise is frequently used in stochastic models to represent random fluctuations in the environment [58]. Heterogeneous diffusion processes (HDPs) with finite-ranged coloured non-Gaussian noise with Tsallis' q -statistical amplitude were recently considered [56]. Here we analyse this process regarding its FPT dynamics. The resulting model is expected to be flexible enough in order to describe FPT dynamics in heterogeneous systems driven by non-standard noise. Our study thus combines the increasing interest in effects encoded by correlated noise on stochastic dynamical systems [40–42] with those stemming from HDP statistic and non-Gaussianity of the driving noise.

When the noise is white and Gaussian HDPs are Markovian, and analytical results can be obtained from the associated Fokker–Planck equation (FPE) in a given stochastic interpretation [59, 60]. For coloured non-Gaussian noise, the process is non-Markovian and thus difficult to solve analytically [61]. However, the problem can be transformed into a two-dimensional Markovian process that describes the joint dynamics of the stochastic process itself and the noise process. An effective Markov FPE can be obtained from approximative approaches, including path integral methods [62, 63] and the unified coloured noise approximation [63, 64]. The second-order moment method can be applied to analyse non-Gaussian noise-driven stochastic systems [65]. Studies using coloured non-Gaussian noise found that the departure of the noise from a Gaussian statistic significantly affects the response of the system, e.g., it enhances the signal to noise ratio in stochastic resonance, current and efficiency in Brownian motors, trapping in resonant gating, and shifts noise-induced transition lines [66–68]. Furthermore, the interaction of different types of noises may lead to peculiar dynamical behaviours [69, 70].

Several studies have considered the FPT problem in multi-state and periodic potentials driven by non-standard noise [71–80], while the barrier crossing problem in the presence of coloured noise has been considered in [81]. The FPT behaviour for a stochastic system driven by correlated noises has been explored in [40, 75, 82]. Although the FPT problem arises frequently in various real systems for which the embedding medium is often heterogeneous most studies in this area ignore the medium's heterogeneity. Yet heterogeneity effects are expected to significantly influence the transport properties. The FPT dynamics for diffusive particle in heterogeneous medium has been considered to some extent in [47, 83–88]. Given the relevance of HDPs with spatially varying diffusivity as well as the expected influence of the driving noise, it is imperative to study the FPT behaviour for particles driven by correlated white Gaussian and non-Gaussian coloured noise in heterogeneous media.

Here, we study the FPTD and MFPT to HDPs with position dependent diffusivity under the conspirative driving of correlated additive white Gaussian and non-Gaussian coloured noise with adjustable strengths. We assume that the coloured non-Gaussian noise follows Tsallis' q -distribution and exhibits an exponential self-correlation. We consider three functional forms for the diffusivity $D(x)$, power-law, exponential, and logarithmic. Practically, particle tracks are numerically simulated and the FPTs recorded, and from these the FPTD and MFPT calculated. The influence of the noise intensity and self-correlation of the multiplicative noise, the intensity of the additive noise, the cross-correlation strength, and the non-extensivity parameter of the q -noise on the MFPT are examined. The paper is organised as follows. In section 2 we provide details on the governing equations. In section 3 we present and discuss the results. Specifically, the simulations results for the FPTD and MFPT are presented, and then the effect of the parameters on the MFPT is analysed. In section 4 we present our conclusions.

2. Model description

2.1. Aspects of the model

Before introducing the dynamic equations in our diffusion model for heterogeneous media driven by non-standard noise we first briefly address the different aspects of the generalised noise source.

The concept of *coloured noise* with an exponential noise–noise correlation and thus *finite* correlation time has a quite long tradition in the theory of stochastic processes [89–92] and was originally considered in connection with laser physics and magnetic resonance phenomena [92–95]. More recent applications of coloured noise include population dynamics [96] or neuron models [97]. Exponentially correlated noise is usually generated by an Ornstein–Uhlenbeck process [57, 98, 99]. Such a noise process depends on two parameters, the correlation time and the noise intensity. In the limit of zero correlation time, the autocorrelation function approaches the delta function of white noise [100]. The distribution of coloured noise is typically assumed to be Gaussian. Coloured noise is thus different from long-range correlated fractional Gaussian noise [101, 102] or fractional Gaussian noise with different form of tempering [103, 104], all of which are characterised by a continuous spectrum of time scales.

We model *non-Gaussian noise* in terms of the Tsallis q -Gaussian or q -distribution [105, 106]. This distribution follows from Tsallis’ non-extensive entropy definition [107, 108] and arises as solution of non-linear FPEs [109]. Such types of distributions were identified in a wide variety of systems, such as financial markets [110, 111], granular media [53], or earthquake statistics [112]. The q -Gaussian emerges as a limit of highly correlated random variables [113]. Such non-extensive characteristics sometimes concurrently also exhibit long correlations or memory [61], a noise type called coloured non-Gaussian noise. Non-Gaussian coloured noise can be viewed as a generalisation of the Ornstein–Uhlenbeck noise with a non-extensivity parameter q indicating the degree of departure from the Gaussian statistic [62, 67].

Different concepts exist to describe heterogeneous media including two or multiple different, quenched layers with different diffusivities, e.g., considered in the modelling transport of proteins between the cell cytoplasm and the interior of the nucleus [114, 115] or the bacterial nucleoid [11, 46], facilitated diffusion including diffusion in one and three dimensions [116, 117], motion in the bulk and ER of live cells [118, 119], lipid motion in protein-crowded membranes [51, 120], particle diffusion with pronounced boundary interactions [121–123], patchy landscapes with different diffusivities [124–127] as well as in quenched, rugged energy landscapes [128, 129], and the ‘diffusing diffusivity’ model [86, 130–136], in which the stochastic motion is modulated by a time-dependent, stochastic diffusion coefficient. In many other situations, the diffusion coefficient may vary systematically as some prescribed function $D(x)$, i.e., in ‘deterministic heterogeneity’ [59, 137–139]. A prime example for the latter behaviour is the diffusivity landscape mapped out in mammalian HeLa and NLFK cells, in which the local diffusivity of the tracers follows a quite clear increase from the cell boundary towards the cell nucleus [6], see also the study for bacteria cells in [140]. Concrete functional forms for $D(x)$ in theoretical studies are typically taken as power-law dependencies as well as logarithmic and exponential variations [59, 141–144]. Whether the medium heterogeneity is deterministic or random, it can significantly influence the FPT dynamics [47, 59, 87, 88, 145].

2.2. Dynamic equations

In the following we consider the system of dynamic equations for the one-dimensional particle displacement $x(t)$ driven by correlated multiplicative coloured non-Gaussian noise $\eta(t)$ (‘ q -noise’ [68]) and additive Gaussian noise $\epsilon(t)$,

$$\frac{dx(t)}{dt} = \sqrt{2D(x)} \times \eta(t) + \epsilon(t), \quad (1)$$

$$\frac{d\eta(t)}{dt} = -\frac{1}{\tau} \frac{d}{d\eta} V_q(\eta) + \frac{1}{\tau} \xi(t). \quad (2)$$

In the Ornstein–Uhlenbeck-type process (2) encoding the coloured noise $\eta(t)$ the driving term $\xi(t)$ represents Gaussian white noise of zero mean and autocorrelation function $\langle \xi(t)\xi(s) \rangle = 2D\delta(t-s)$. Similarly, $\langle \epsilon(t)\epsilon(s) \rangle = 2Q\delta(t-s)$ for the noise $\epsilon(t)$. However, these two noises are not independent of each other but correlated in the form $\langle \epsilon(t)\xi(s) \rangle = \langle \xi(t)\epsilon(s) \rangle = 2\lambda\sqrt{DQ}\delta(t-s)$ where λ quantifies the cross-correlation strength taking on value in the interval $[-1, 1]$. In the limit $\lambda = 0$ the two noise sources are uncorrelated, while for $-1 \leq \lambda < 0$ and $0 < \lambda \leq 1$ the two noise sources are negatively and positively correlated, respectively. D and τ are the noise intensity and characteristic time (self-correlation time) of the multiplicative coloured non-Gaussian noise $\eta(t)$. Moreover Q is the strength of the additive Gaussian noise $\epsilon(t)$, and the q -noise potential $V_q(\eta)$ is given by

$$V_q(\eta) = \frac{1}{\beta(q-1)} \log \left[1 + \beta(q-1) \frac{\eta^2}{2} \right] \quad (3)$$

with $\beta = \tau/D$. The non-extensivity parameter q indicates the departure from Gaussian behaviour ($q = 1$). Note that when $Q = 0$ and $\lambda = 1$ the system is driven purely by non-Gaussian coloured noise. It is important to note that equations (1) and (2) constitute Brownian dynamics which is a simplified form of Langevin dynamics corresponding to the overdamped limit in absence of inertia effects [146].

Finally the diffusion coefficient in equation (1) is position dependent, and we will explore the FPT dynamics for three forms of the functional dependence of the diffusivity: power-law, exponential and logarithmic. Concretely, for the power-law form $D(x) = D_0|x|^\alpha$ with scaling exponent α several recent studies considered diffusivities with either constant or variable power-law exponent [57, 142]. To avert trapping of the particle due to the singularity at the origin $x = 0$ (zero or diverging diffusivity, depending on the value of α) in our simulations we consider the diffusivity of the form

$$D(x) = \begin{cases} D_0(a + |x|^\alpha), & \text{for } \alpha > 0, \\ D_0/(a + |x|^\alpha), & \text{for } \alpha < 0, \end{cases} \quad (4)$$

with sufficiently small offset a [59, 142]. The exponent α assumes real values. The diffusivity is a constant for $\alpha = 0$, which implies a homogeneous diffusion process. For $\alpha > 0$, the diffusivity increases with increasing $|x|$, and conversely for $\alpha < 0$. For the exponential and logarithmic dependencies we consider diffusivities of the form

$$D(x) = \frac{D_0^2}{2} \exp(-2\alpha x) \quad (5)$$

and

$$D(x) = \frac{D_0^2}{2} \log(x^2 + 1), \quad (6)$$

respectively. We interpret the stochastic integral corresponding to the Langevin equation (1) in the Stratonovich sense [59]. This interpretation is permitted as long as we do not require the system to reach equilibrium, e.g., on a finite domain or in a confining external potential while coupled to a thermostat [60, 139, 147]. Moreover, the motion of tracers in biological cells, spreading patterns of animals or humans, or dynamics in financial mathematics are typically far from equilibrium. Other conventions for the stochastic interpretation such as Itô and Hänggi–Klimontovich can be included in the numerical analyses [60]. It should be pointed out that, although the multiplicative term in equation (1) represents the diffusion profile, it can be viewed as an effective potential profile.

Note that the q -noise (2) is a generalisation of the Ornstein–Uhlenbeck process which renders the system non-Markovian. The statistical properties of the noise process $\eta(t)$ were discussed in [62, 68]. By solving the corresponding FPE the stationary distribution $P_q^{\text{st}}(\eta)$ can be obtained. $P_q^{\text{st}}(\eta)$ is well defined only for $q \in (-\infty, 3)$ while for $q \geq 3$ it is not normalisable and thus not a valid PDF. To show this, we note that for $q \in (1, 3)$ the stationary distribution reads

$$P_q^{\text{st}}(\eta) = \frac{1}{Z_q} \left[1 + \beta(q-1) \frac{\eta^2}{2} \right]^{-1/(q-1)}, \quad \eta \in (-\infty, \infty), \quad (7)$$

with normalisation factor $Z_q = [\pi/(\beta(q-1))]^{1/2} \Gamma(1/[q-1] - 1/2) / [\Gamma(1/[q-1])]$, where Γ indicates the Gamma function. For $q = 1$ we then get

$$P_1^{\text{st}}(\eta) = \frac{1}{Z_1} \exp(-\beta n^2/2), \quad (8)$$

with normalisation factor $Z_1 = \sqrt{\pi/\beta}$. This expression corresponds to the regular Ornstein–Uhlenbeck process⁴.

Moreover for $q \in (-\infty, 1)$ the stationary PDF is given by

$$P_q^{\text{st}}(\eta) = \begin{cases} \frac{1}{Z_q} \left[1 - \left(\frac{\eta}{w} \right)^2 \right]^{1/(1-q)}, & \text{if } |\eta| < w, \\ 0, & \text{otherwise,} \end{cases} \quad (9)$$

with normalisation factor $Z_q = \sqrt{\pi/(\beta(1-q))} \Gamma(1/(1-q) + 1) / \Gamma(1/(1-q) + 3/2)$. Here $w = [(1-q)\beta/2]^{-1/2}$ is a cutoff value. Thus the stationary distribution indeed exists only for $q < 3$ —since for $q \geq 3$, Z_q diverges or it is negative and consequently $P_q^{\text{st}}(\eta) < 0$ and thus not a PDF. The Ornstein–Uhlenbeck process,

⁴ Note that the Ornstein–Uhlenbeck process can directly be recovered from equation (2) by setting $q = 1$. First differentiating equation (3) with respect to η , which produces $\eta/[1 + \beta(q-1)\eta^2/2]$, then setting $q = 1$ yields $dV_q/d\eta = \eta$; thus the drift term in equation (2) is $-\eta/\tau$.

i.e., the process giving rise to Gaussian coloured noise, is recovered in the limit $q \rightarrow 1$. For $1 < q < \frac{5}{3}$ the distribution is fat-tailed while $q < 1$ yields cut-off distributions. The first moment vanishes, $\langle \eta(t) \rangle = 0$, while the second moment is finite only when $q < \frac{5}{3}$, for which it reads $\langle \eta(t)^2 \rangle = 2D/[\tau(5 - 3q)]$.

Here, we use a discrete representation based on fourth-order Runge–Kutta-type integration to simulate the particle trajectories. Appendix A presents the numerical discretisation scheme. Particles are released from the origin and then their FPTs to $x = L = 10$ are recorded. The motion is terminated when the particle reaches $x = L$ while at the point $x = -L = -10$ they are reflected.

3. Results and discussions

We now proceed to the analysis of the FPT problem for the stochastic process defined by equations (1) and (2) using numerical simulations.

3.1. Position-dependent diffusivity of power-law form

Figure 1 shows the FPTD for different values of the non-extensivity parameter q , and with varying noise–noise coupling strength λ and scaling exponent α of the position-dependent diffusion coefficient varied horizontally and vertically between the panels, respectively. The curves of the PDFs are non-monotonic and have maxima at short times, indicating that the probability of reaching the absorbing boundary is more concentrated around short FPT. For $q = 1.0$, the peak value moves to the right and the FPTD broadens with increasing λ . For $q = 0.1$ and 1.5 , the FPTDs are almost the same for $\lambda = 0$ and 0.5 but we see a broadening when $\lambda = 1$. The MFPT increases with increasing λ , see the vertical lines in the colours representing the respective MFPT. When $\lambda = 0$ or 0.5 the height of maxima is higher and lower for $q = 1.0$ and 0.1 , respectively, compared to the one for $q = 1.5$. Concurrently, for $\lambda = 1$ the height of maxima is higher and lower for $q = 1.5$ and 1.0 , respectively compared to the one for $q = 0.1$, and the PDFs exhibit longer right tails. We note that the tails may be attributed to extreme values or outliers. As shown by the MFPTs represented by the vertical lines it is such long FPT events that define the MFPT. In a finite number of measurements the empirical or *typical MFPT* is thus expected to be shorter than the MFPT obtained from a sufficiently large sample, see also the discussion in [148].

For fixed λ and q , the PDFs in figure 1 exhibit almost the same behaviour, but the heights of their maxima and the widths vary with α . Long FPTs may arise due to slow or retarded motion of the particles or due to back-and-forth movement causing a delay. In contrast, short FPTs imply more directed movement. These observations correspond to the idea of geometry-controlled dynamics, i.e., the most likely FPT is close to the time $\langle x^2(t_0) \rangle = L^2$ for passing (almost) directly from the initial position to the absorbing boundary [10, 12]. Using the closed form for the MSD [56]

$$\langle x^2(t) \rangle = \frac{\Gamma(p + \frac{1}{2})}{\sqrt{\pi}} \left[\sqrt{D_0 D_q} \frac{2}{p} \left(\frac{2-q}{5-3q} \right) \right]^{2p} t^p, \quad (10)$$

where $p = 2/(2-\alpha)$, this means that the most likely FPT for such ‘direct trajectories’ [10, 12] scales like $t_0 \simeq L^{2/p}$. Naively, we would expect α to affect the FPTD strongly, but for finite noise–noise cross-correlation coupling the influence of α appears to be mitigated. The case of $\alpha = 0$ and $q \approx 1$, represented by the red dashed line in the middle panels, corresponds to the FPTD of homogeneous Brownian motion-driven correlated multiplicative coloured Gaussian and additive white noises. We note that departure from Gaussianity significantly influences the FPT behaviour.

The coefficient of variation (CV) measures the relative variation within a data set, i.e., the dispersion of the distribution. It is the ratio of the standard deviation to the mean, for the FPTs t this implies

$$CV = \frac{\sqrt{\langle t^2 \rangle - \langle t \rangle^2}}{\langle t \rangle}, \quad (11)$$

where the denominator is the MFPT. A low CV value means relatively little variation within the distribution while a high CV implies larger variation. Generally, when CV exceeds unity, meaning that the standard deviation is larger than the mean, the underlying distribution is ‘broad’ in the sense that the average (here the MFPT) is not representative of the actual behaviour of a single realisation, see the discussion in [10, 12, 149].

If sampled from a normally distributed population an unbiased estimator for the CV is

$$CV^* = \left(1 + \frac{1}{4n} \right) \times CV, \quad (12)$$

where n is the sample size (i.e., the number of observations). For distributions deviating from the normal distribution more accurate estimators may be used. In particular, for log-normally distributed data, the estimator

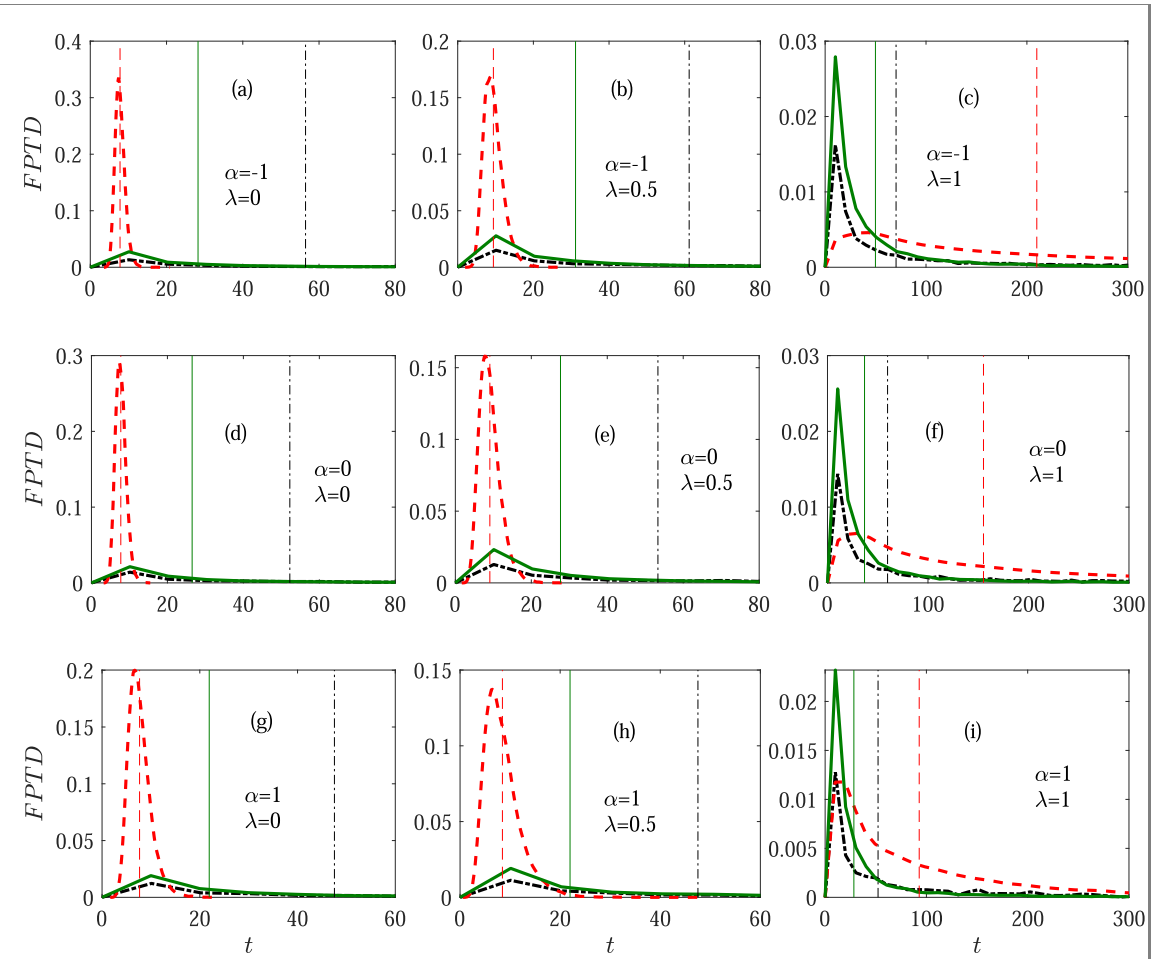


Figure 1. FPTD for different values of the non-extensivity parameter q ($q = 0.1$: black dash-dotted line; $q = 1$: red dashed line; $q = 1.5$: green solid line). The noise–noise coupling strength λ varies across the figure as $\lambda = 0, 0.5$, and 1 from left to right, while α varies from top to bottom as $\alpha = -1, 0$, and 1 . In all panels we use the parameters $D = 0.5$, $Q = 0.5$, $D_0 = 0.01$, $\tau = 0.1$, and $M = 1 \times 10^4$. The initial position of the particles is at the origin. The dashed vertical lines in the corresponding colours represent the respective MFPT.

becomes

$$\text{CV}_{\text{LN}} = \sqrt{\exp(s_{\text{LN}}^2) - 1}, \quad (13)$$

where s_{LN}^2 is the variance of the logarithm of the data. A 95% confidence interval of CV is given by

$$\text{CV} \pm t_{\alpha^*, n-1} \text{SE}(\text{CV}^*), \quad (14)$$

where $\text{SE}(\text{CV}^*) = \text{CV}(1 + 1/(4n))/\sqrt{2n}$ is the standard error of CV corrected for bias. Here $t_{\alpha^*, n-1}$ is the upper $(1 - \alpha/2)$ -critical value for the t -distribution with $(n - 1)$ degrees of freedom, and α^* represents the level of significance with confidence level given by $(1 - \alpha^*)$.

The CV for the FPTD as a function of the non-extensivity parameter q is shown in figure 2. The lowest and highest values are reached when $q = 1$ and 0.9 , respectively. CV first remains fairly constant, with a shallow descent before spiking to its maximum at $q = 0.9$, dropping to the minimum value at $q = 1$, and then increasing to what appears like a plateau. While for $q < 0.9$ the CV value is almost the same for all values, the plateau value at $q > 1.0$ depends somewhat on the noise–noise coupling strength λ . To see the dependence on the diffusivity scaling exponent α note the different ranges of CV in the three panels. In particular the maximum at $q = 0.9$ increases with increasing α . The overall behaviour is, however, quite similar for all α . In all cases we note that CV reaches values far above unity. Consequently the MFPT is far less than the standard deviation and thus not a sufficient measure to account for the full FPT statistic, apart from the case $q \approx 1.0$, i.e., the Gaussian case. The CV suggests a broad FPTD for $q \neq 1$, which is indeed observed in figure 1.

Figure 3 depicts the variation of the MFPT with the non-extensivity parameter q for different values of the diffusivity scaling exponent α and the noise–noise coupling strength λ . For $\lambda = 0$ or 0.5 (panel (a)) the MFPT first shows a fairly gradual growth and then drops to a minimum at $q = 0.9$, before then increases with growing q . For $|\lambda| = 1$ (panel (b)) the MFPT exhibits an additional spike at $q = 1$ and has a minimum for $q > 1$. For fixed q , the MFPT is lowest and highest for $\alpha = 1$ and -1 , respectively, compared to the MFPT when $\alpha = 0$.

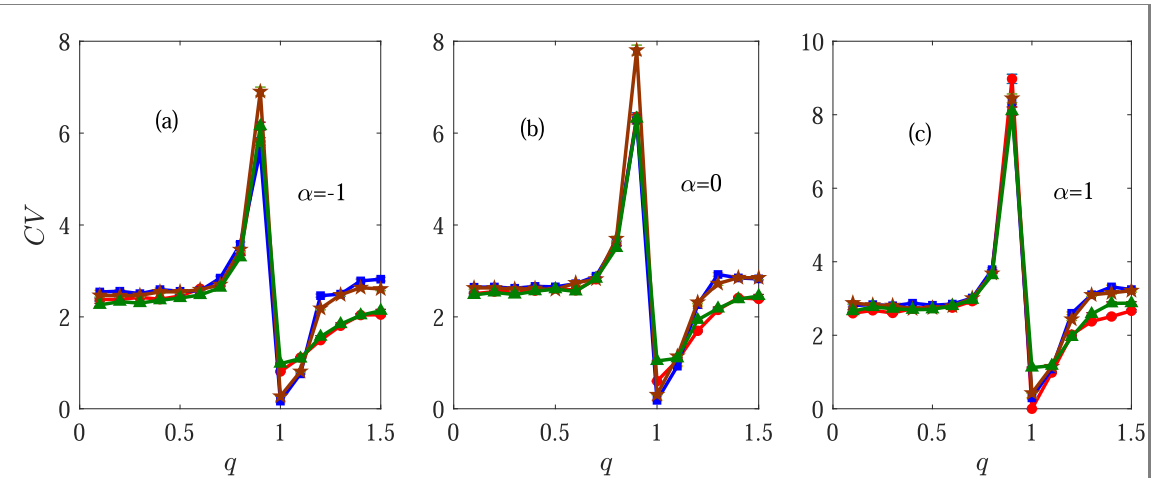


Figure 2. CV (11) for the FPTD as a function of the non-extensivity parameter q for different values of the noise–noise coupling strength λ . The diffusivity scaling exponent α varies across the figure as $\alpha = -1, 0$, and 1 . The solid lines with the circle, square, pentagon, and triangle are for $\lambda = -1, 0, 0.5$ and 1 , respectively. In all panels the parameters are $D = 0.5$, $Q = 0.5$, $D_0 = 0.01$, $\tau = 0.1$, and $M = 1 \times 10^4$. The initial position of particles is at the origin. Error bars according to relation (14) are also displayed but are of the size of the symbols.

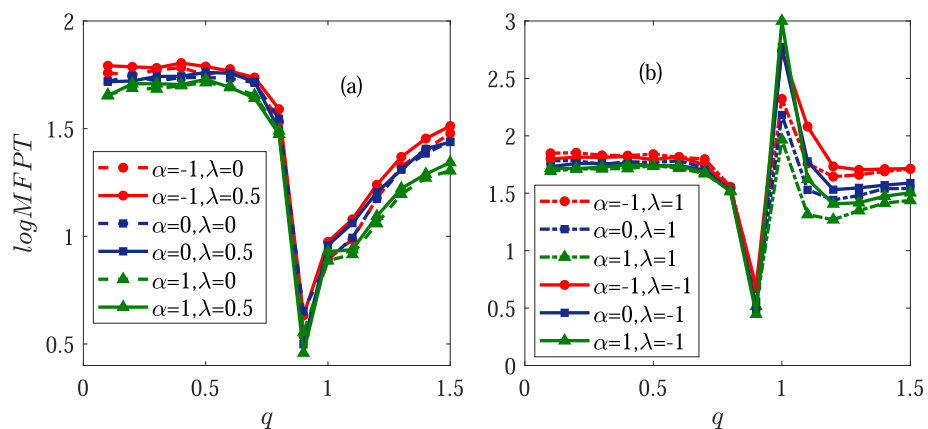


Figure 3. MFPT as a function of the non-extensivity parameter q for various values of the diffusivity scaling exponent α and the noise–noise coupling strength λ . In all panels we chose the parameters $D = 0.5$, $Q = 0.5$, $D_0 = 0.01$, $\tau = 0.1$, and $M = 1 \times 10^4$. The initial position of the particles is at the origin.

For $q < 0.7$ the MFPT remains fairly constant, for $q \geq 1.1$ the MFPT increases, while for $0.7 < q < 1.1$ the behaviour of the MFPT varies in dependence on λ . For $q \leq 0.7$ the MFPT is larger than for $q > 1.1$. Depending on λ the non-Gaussianity q leads to a low or large MFPT. The MFPT exhibits minimum which can be viewed as a resonant activation-like phenomenon. Coloured non-Gaussian noise can be approximated as Gaussian noise (i.e., Ornstein–Uhlenbeck process) with effective noise correlation time τ_{eff} and effective noise intensity D_{eff} given by $\tau_{\text{eff}} = 2(2 - q)\tau/(5 - 3q)$ and $D_{\text{eff}} = [2(2 - q)/(5 - 3q)]^2 D$. Both effective noise strength and effective noise correlation time increase with growing q , but they have opposite effects on the diffusion of a particle. The effective noise strength accelerates the diffusion of a particle, while the effective correlation time retards the diffusion. When $|q - 1|$ is sufficiently small, the coloured non-Gaussian noise departs from Gaussian noise only slightly, but exhibits some of the main trends of non-Gaussian noise. A negative α value inhibits some particles from reaching the absorbing boundary, while a positive α -value promotes particles reaching the absorbing boundary. 95% confidence intervals for the MFPT under different values for q , α , and λ are presented in table 1 in appendix B.

Figure 4 presents the MFPT as a function of the noise–noise coupling strength λ for different values of the non-extensivity parameter q and the diffusivity scaling exponent α . When $q = 0.1$ or 1.5 the MFPT remains fairly constant, with gradual growth as function of $|\lambda|$ for all α . The MFPT for $q = 0.1$ is larger than the one for $q = 1.5$. For the Gaussian case $q = 1.0$ the MFPT increases with increasing $|\lambda|$, i.e., it has a minimum for vanishing noise–noise coupling. A strong growth is seen when λ is close to unity, and the MFPT for $q = 1.0$ crosses the value for $q = 1.5$ and 0.1 . The effect of noise coupling is significant when both the multiplicative

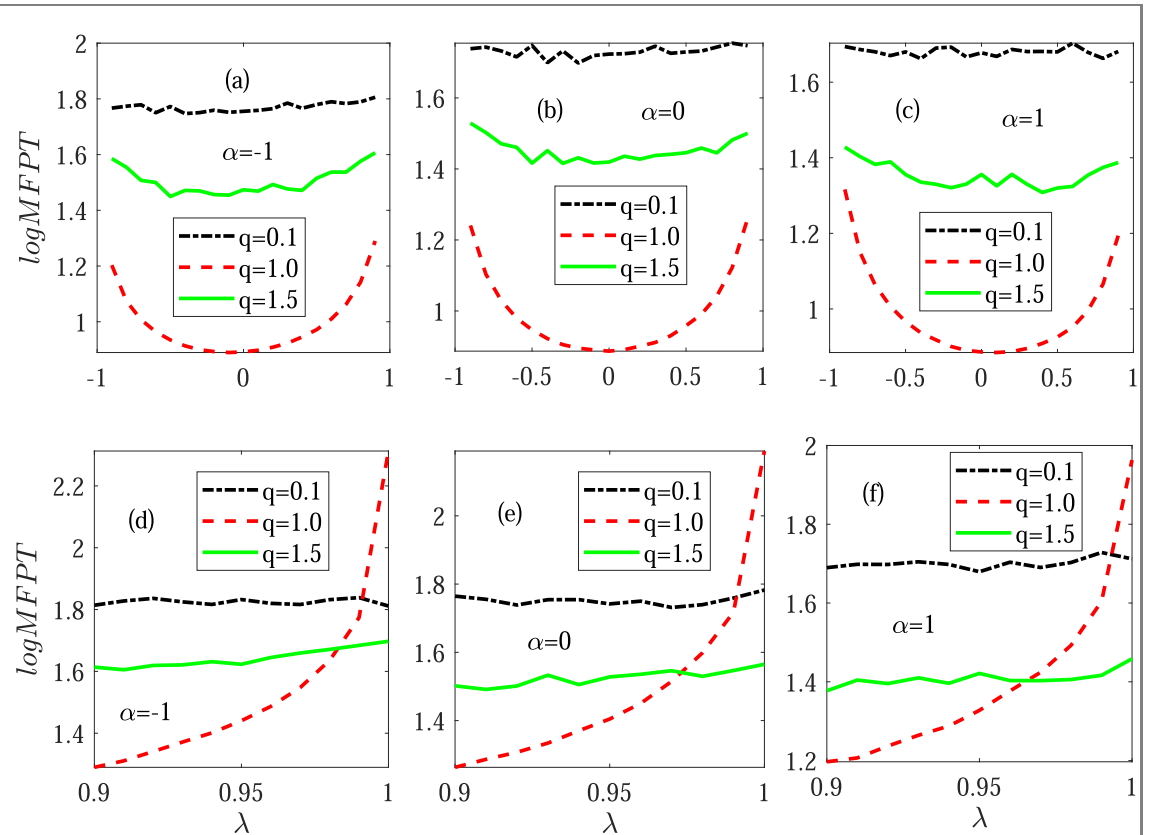


Figure 4. MFPT as a function of the noise–noise correlation strength λ for various values of the non-extensivity parameter q . In all panels $D = 0.5$, $Q = 0.5$, $D_0 = 0.01$, $\tau = 0.1$, and $M = 1 \times 10^4$. The bottom panels show a zoom into the region around $\lambda = 0.95$. The initial position of the particles is at the origin.

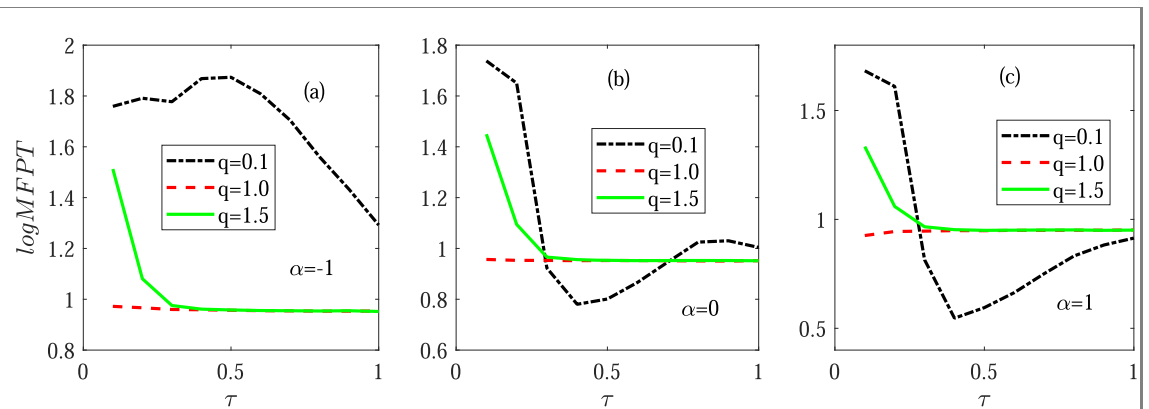


Figure 5. MFPT as function of the self-correlation time τ of the non-Gaussian coloured noise under variation of the non-extensivity parameter q and the diffusivity scaling exponent α . In all panels $D = 0.5$, $Q = 0.5$, $D_0 = 0.01$, $\lambda = 0.5$, and $M = 1 \times 10^4$. The initial position of the particles is at the origin.

and additive noises are Gaussian ($q = 1$), but the effect diminishes when the multiplicative noise departs from Gaussian behaviour.

Figure 5 displays the dependence of the MFPT on the self-correlation time τ of the non-Gaussian coloured noise for different non-extensivity parameters q and diffusivity scaling exponent α . For the Gaussian case $q = 1.0$ the MFPT is insensitive to τ . For $q = 1.5$, with growing τ the MFPT decreases to a plateau, that has the same value for all q , which means that the increase of τ —up to some limiting value—accelerates particles to reach the absorbing boundary. For $q = 0.1$ the MFPT first increases somewhat for $\alpha = -1$ then decreases to a minimum value, before slightly increasing to the common plateau. The MFPT is a non-monotonic function of τ with a minimum, indicating, as mentioned before, a resonant activation-like phenomenon, see also the discussion in [150]. When a small τ is fixed, departure from a Gaussian behaviour leads to large MFPT values. It is also seen that when τ is small, α influences the behaviour of the MFPT.

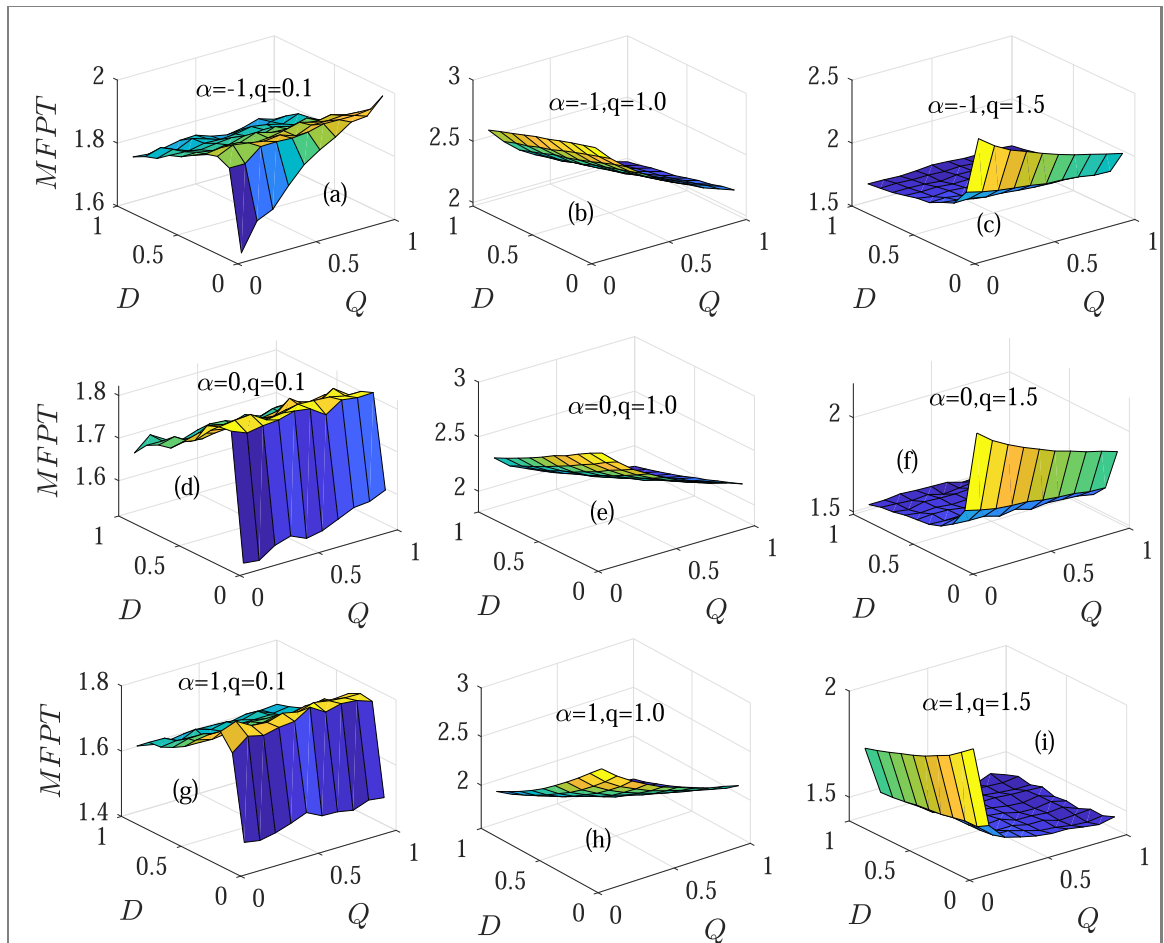


Figure 6. MFPT as function of the intensity D of the multiplicative non-Gaussian coloured noise and strength Q of the additive Gaussian white noise. The non-extensivity parameter q varies horizontally across the figure as $q = 0.1, 1.0$, and 1.5 , while the diffusivity scaling exponent α varies vertically in the figure as $\alpha = -1, 0$, and 1 . In all panels we chose $D_0 = 0.01$, $\lambda = 1$, $\tau = 0.1$, and $M = 1 \times 10^4$. The initial position of the particles is at the origin.

Figure 6 presents the combined effects of the intensity D of the multiplicative non-Gaussian coloured noise and strength Q of the additive Gaussian white noise on the MFPT when the non-extensivity parameter q is varied horizontally across the figure ($q = 0.1, 1.0$, and 1.5) and the diffusivity scaling exponent α varied vertically ($\alpha = -1, 0$, and 1). In panels (a), (d), and (g) (i.e., when $q = 0.1$) the MFPT first increases rapidly and then decreases gradually after passing through a maximum. The MFPT is a non-monotonic function of D , but it remains fairly constant, with gradual growth with growing Q . The MFPT is large when $0.2 < D < 0.5$ and low when D is close to zero. The nonmonotonic dependence of the MFPT on the noise intensity D with a maximum as exhibited in panels (a), (d), and (g) is a signature of a noise enhanced stability (NES)-like phenomenon. We attribute this NES to the temporary presence of a metastable state due to the stochastic potential profile. Enhancement of the stability of a metastable state by noise has indeed been observed in several other systems [151–153]. In panels (b), (e), and (h) (when $q = 1$) the MFPT decreases with growing D or Q . The descent is more shallow with growing D than with growing Q , but it becomes more with increasing α . The highest and lowest MFPT are reached when both D and Q are close to zero and one, respectively. When $q = 1$ increasing D or Q accelerates the approach to the boundary at $x = L$. In panels (c), (f), and (i) ($q = 1.5$) the MFPT descends with decreasing D or Q . In both panels (c) and (f) the descent is rapid and shallow with growing D and Q respectively, while in panel (i) the descent is rapid and shallow with growing Q and D respectively. The MFPT is short when both D and Q are large which means increasing both D and Q accelerate the particle to reach the boundary. The interplay of D and Q significantly influences the MFPT. We note that figures 5 and 6 reveal that D and τ (both parameters for the non-Gaussian noise) conspire in reducing the MFPT.

3.2. Exponential position dependence of the diffusivity

Here, we consider the situation when the diffusion coefficient has the exponential position dependence (5) [142].

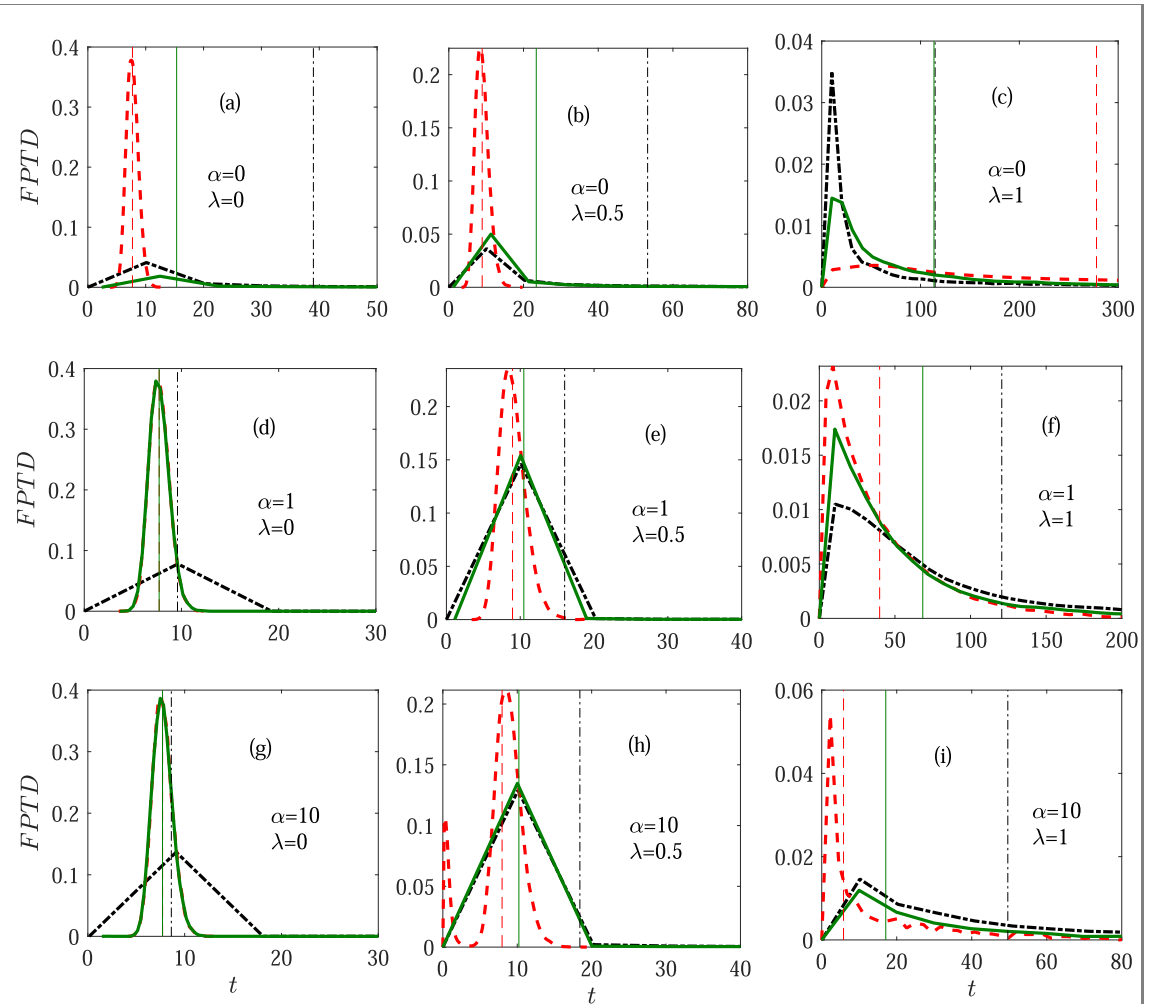


Figure 7. FPTD for different values of the non-extensivity parameter q ($q = 0.1$: black dash-dotted line; $q = 1$: red dashed line; $q = 1.5$: green solid line). The noise–noise coupling strength λ varies horizontally across the figure as $\lambda = 0, 0.5$, and 1 while the diffusivity exponent α varies vertically as $\alpha = 0, 1$, and 10 . In all panels we chose $D = 0.5$, $Q = 0.5$, $D_0 = 0.01$, $\tau = 0.1$, and $M = 1 \times 10^4$. The thin vertical lines in the corresponding line types and colours represent the respective MFPT. The initial position of the particles is at the origin.

Figure 7 shows the FPTD for different values of the non-extensivity parameter q , with variation of the noise–noise coupling strength λ and the diffusivity exponent α horizontally and vertically across the figure, respectively. The curves of the PDFs are non-monotonic with maxima at short times. The FPTDs exhibit long right tails and broaden with increasing λ . Concurrently, the MFPT increases with growing λ . The MFPT is to the right of the peak of the FPTD, implying that the tail of long FPTs dominate the MFPT value. For a fixed q and λ the FPTDs exhibit similar behaviours but the peaks and the MFPT vary with α . An exception to this observation is noted in figure 7(h) for $q = 1$, where the PDF has two peaks. The peaks of PDFs and the MFPT vary with q , α , and λ .

Figure 8 shows the CV of the FPTD as function of the non-extensivity parameter q for different values of the noise–noise coupling strength λ . For $\alpha = 0$, when $\lambda = 0, 0.5$, or 1 the CV first decreases to a minimum value and then increases to what appears like a plateau with growing q . When $\lambda = -1$ the CV first remains fairly constant slightly above one, drops to a minimum value, and then increases to a plateau below one with increasing q . q less or greater than the critical value yields CV values significantly exceeding one. For $\lambda = -1, 0$, and 0.5 the CV is minimal when $q = 1$ and it is less than one, while for $\lambda = 1$ it is minimal when $q = 0.9$. The case that $\alpha = 0$ represents a homogeneous environment, but figures 2(b) and 8(a) show a somewhat different trend, which can be attributed to the diffusion coefficient, which is $D_0(a + 1)$ and $D_0^2/2$ in the former and latter cases, respectively. For $\alpha = 1$ the CV first remains fairly constant, with gradual growth, then steps up at $q = 0.9$, and drops to a minimum value at $q = 1$, before increasing to a plateau with growing q . When $1.0 \leq q \leq 1.1$ the CV is less than one, otherwise the CV significantly exceeds one. When $\alpha = 10$ the CV for $\lambda = -1$ and 1 first remains fairly constant with gradual growth, drops to a minimum value at $q = 0.9$, and then decreases gradually to a constant for $\lambda = -1$ and increases to a plateau for $\lambda = 1$ with growing q . For $\lambda = 0$ and 0.5 the CV first increases gradually, drops to the minimum value at $q = 1$, then remains constant

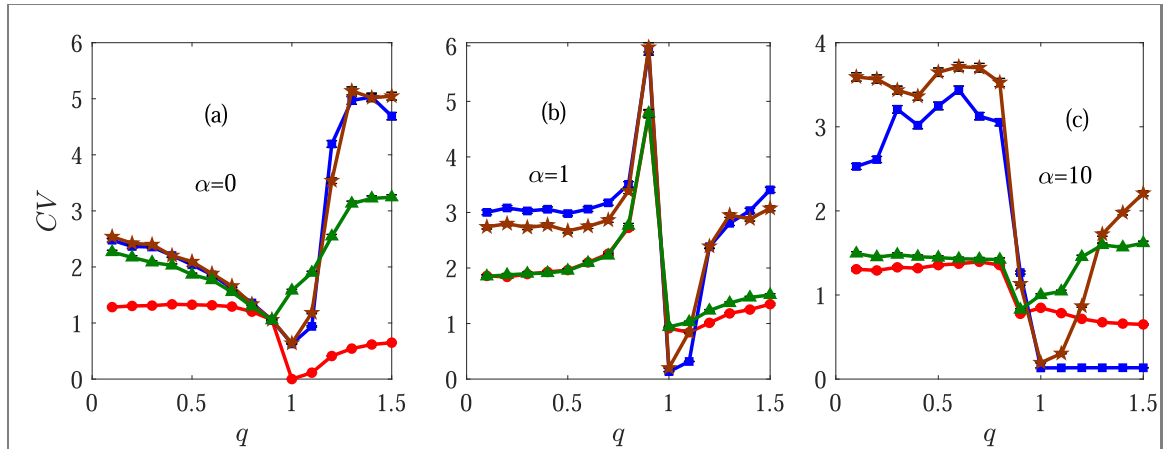


Figure 8. CV of the FPTD as function of the non-extensivity parameter q for different values of the noise–noise coupling strength λ . The value of the diffusivity exponent α is varied across the panels as $\alpha = 0, 1$, and 10 . Solid lines and symbols represent $\lambda = -1$ (circles), $\lambda = 0$ (squares), $\lambda = 0.5$ (pentagons), and $\lambda = 1$ (triangles). In all panels we chose $D = 0.5$, $Q = 0.5$, $D_0 = 0.01$, $\tau = 0.1$, and $M = 1 \times 10^4$. The initial position of the particles is at the origin. Error bars are of the size of the symbols.

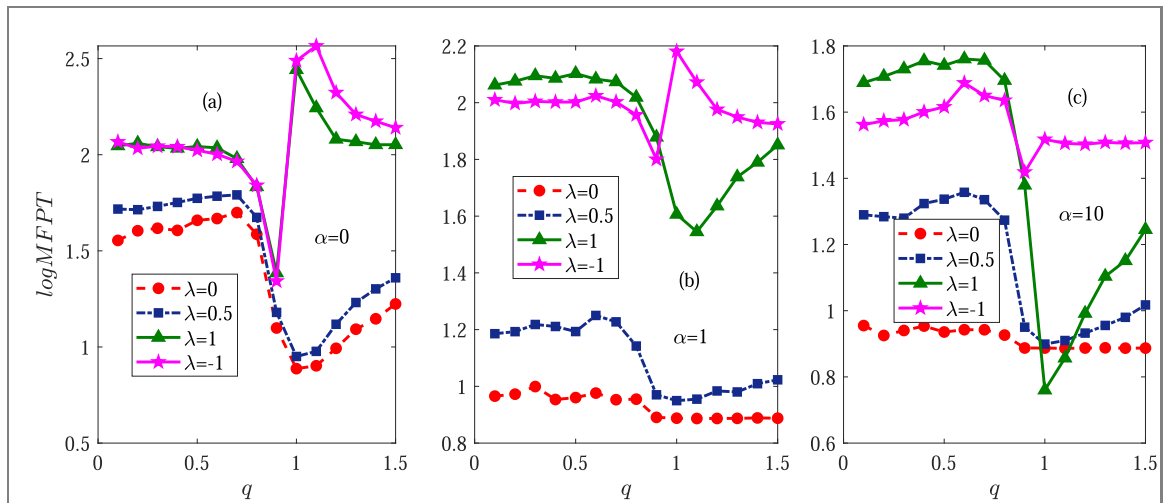


Figure 9. MFPT as a function of the non-extensivity parameter q for various values of the diffusivity exponent α and the noise–noise coupling strength λ . In all panels we chose $D = 0.5$, $Q = 0.5$, $D_0 = 0.01$, $\tau = 0.1$, and $M = 1 \times 10^4$. The initial position of the particles is at the origin.

for $\lambda = 0$ and increases to a plateau for $\lambda = 0.5$, with growing q . In all cases the CV is lower than unity at the critical q . Note that when the CV significantly exceeds unity, this indicates a large variation in the FPTD, i.e., the MFPT may not be a good representative of single trajectory FPTs.

Figure 9 displays the MFPT as a function of the non-extensivity parameter q for various values of the diffusivity exponent α and noise–noise coupling strength λ . The MFPT is a non-monotonic function of q and exhibits a minimum, which again indicates a resonant activation-like phenomenon. With increasing q the MFPT first increases gradually, before descending to the minimum value and then increases or remains fairly constant. For $|\lambda| = 1$ and $\alpha = 0$, and for $\lambda = -1$ and $\alpha = 1$, after its minimum the MFPT increases to a maximum value and then descends to what appears like a plateau. For $\lambda = 0$ and 0.5 the MFPT is lowest when q is close to one (i.e., when the noise tends to coloured Gaussian noise), while for $|\lambda| = 1$, depending on α , the lowest MFPT occurs either when $q = 0.9$ or 1 . For fixed α and λ the interplay between effective noise intensity and the effective noise correlation time of the multiplicative noise influence the MFPT. Both the effective noise intensity and the effective noise correlation time increase with increasing q . 95% confidence intervals for the MFPT for different values of q , α , and λ are presented in table 2 in appendix B.

Figure 10 depicts the MFPT as function of the noise–noise coupling strength λ for different values of the non-extensivity parameter q , while the diffusivity exponent α varies across the figure. In all panels the minimum MFPT occurs when $\lambda = 0$. The MFPT increases with increasing $|\lambda|$, except for $q = 1.0$ when $\alpha = 10$, where the MFPT decreases with increasing λ . For $\alpha = 0$ the MFPT is approximately symmetric in λ with respect to $\lambda = 0$. In contrast, for $\alpha = 1$ and 10 the MFPT is lower for negative λ compared to positive λ . When $\alpha = 1$ or 10 , for negative λ the MFPTs for $q = 1$ and 1.5 are almost the same. When $\alpha = 0$ and λ is close to

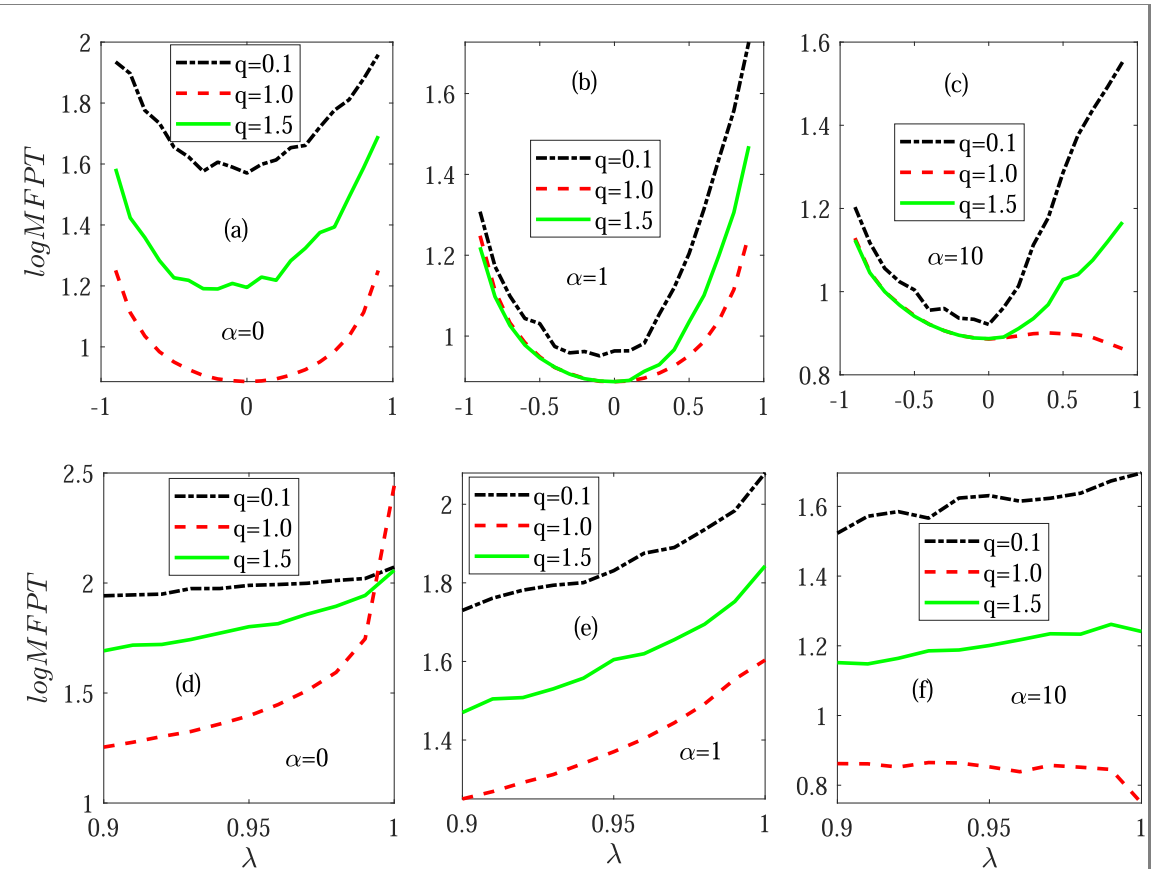


Figure 10. MFPT as a function of the noise–noise coupling strength λ for various values of the non-extensivity parameter q . The diffusivity exponent α is varied across the figure. In all panels we chose $D = 0.5$, $Q = 0.5$, $D_0 = 0.01$, $\tau = 0.1$, and $M = 1 \times 10^4$. The initial position of the particles is at the origin.

unity, the MFPT for $q = 1$ exhibits a rapid growth. For fixed $|\lambda|$ long and short MFPTs occur when $q = 0.1$ and 1.0, respectively. Generally non-Gaussianity $q \neq 1$ leads to a large MFPT. The noise coupling inhibits some particles from reaching the absorbing boundary, but the effect of q and α can modify this behaviour, as seen in figures 10(c) and (f) when $q = 1.0$.

Figure 11 displays the dependence of the MFPT on the self-correlation time τ of the multiplicative coloured noise for various values of the non-extensivity parameter q , while the diffusivity exponent α varies horizontally across the figure. For $q = 1.0$, the MFPT remains constant with increasing τ , but when $\alpha = 10$ and τ is small the MFPT exhibits gradual growth. Concurrently, for $q = 0.1$ and $q = 1.5$ the MFPT first decreases and then remains constant (matching the MFPT for $q = 1.0$) with increasing τ . For fixed, small τ the MFPT is long, and short for $q = 0.1$ and 1.0, respectively. Moreover the MFPT drops with increasing α . For large τ values the MFPTs for all q coincide, which means that non-Gaussian and Gaussian coloured noise leads to almost the same MFPT. When τ is small, departure from Gaussianity inhibits some particles from reaching the absorbing boundary, and the effect is more pronounced when $q < 1$ compared to $q > 1$.

Figure 12 presents the conspirative effect of the noise intensity D of the multiplicative non-Gaussian coloured noise and the strength Q of the additive Gaussian white noise on the MFPT. Here the non-extensivity parameter q is varied horizontally ($q = 0.1$, 1.0, and 1.5) while the diffusion exponent α is varied vertically ($\alpha = 0, 1$, and 10). In panel (a) the MFPT is large when D and Q are both close to zero. The MFPT in panel (a) decreases gradually with increasing D while it is a non-monotonic function of Q (particularly for D close to one), first increasing gradually to a maximum value and then descending with increasing Q , a signature of an NES-like phenomenon. The MFPT decreases gradually with increasing D while it is a non-monotonic function of Q , first increasing gradually to a maximum value and then descending with growing Q , which is similar to the resonant activation phenomena. In the other panels the MFPT increases significantly when Q becomes small. The effect of D is more moderate, but generally the MFPT increases with decreasing D . With the increase of D or Q particle is accelerated to reach the absorbing boundary.

3.3. Logarithmic position dependence of the diffusivity

We now turn to the final case in which the diffusion coefficient has the logarithmic dependence (6) on the position [142].

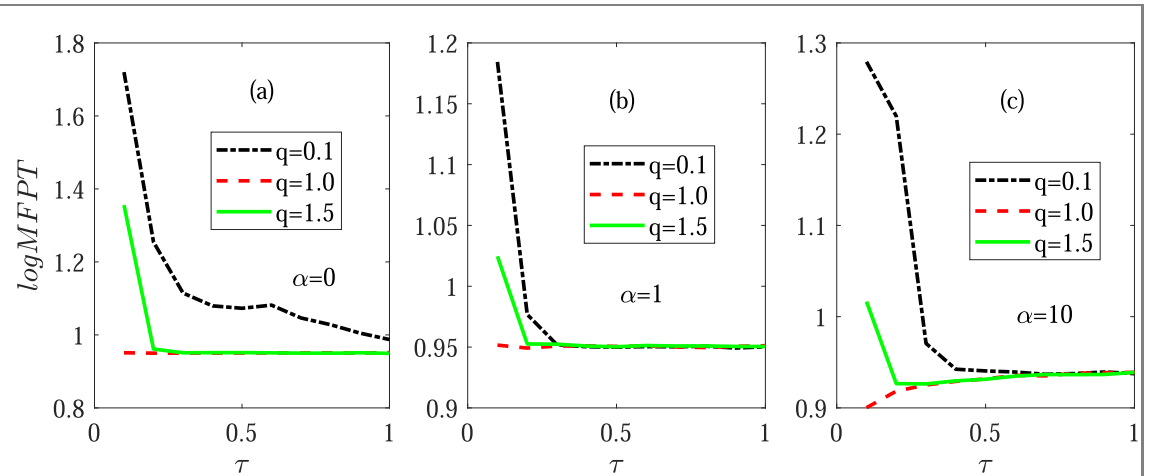


Figure 11. MFPT as function of the self-correlation time τ of the multiplicative coloured noise, for various values of the non-extensivity parameter q . The diffusivity exponent α varies across the panels. In all panels we chose $D = 0.5$, $Q = 0.5$, $D_0 = 0.01$, $\lambda = 0.5$, and $M = 1 \times 10^4$. The initial position of the particles is at the origin.

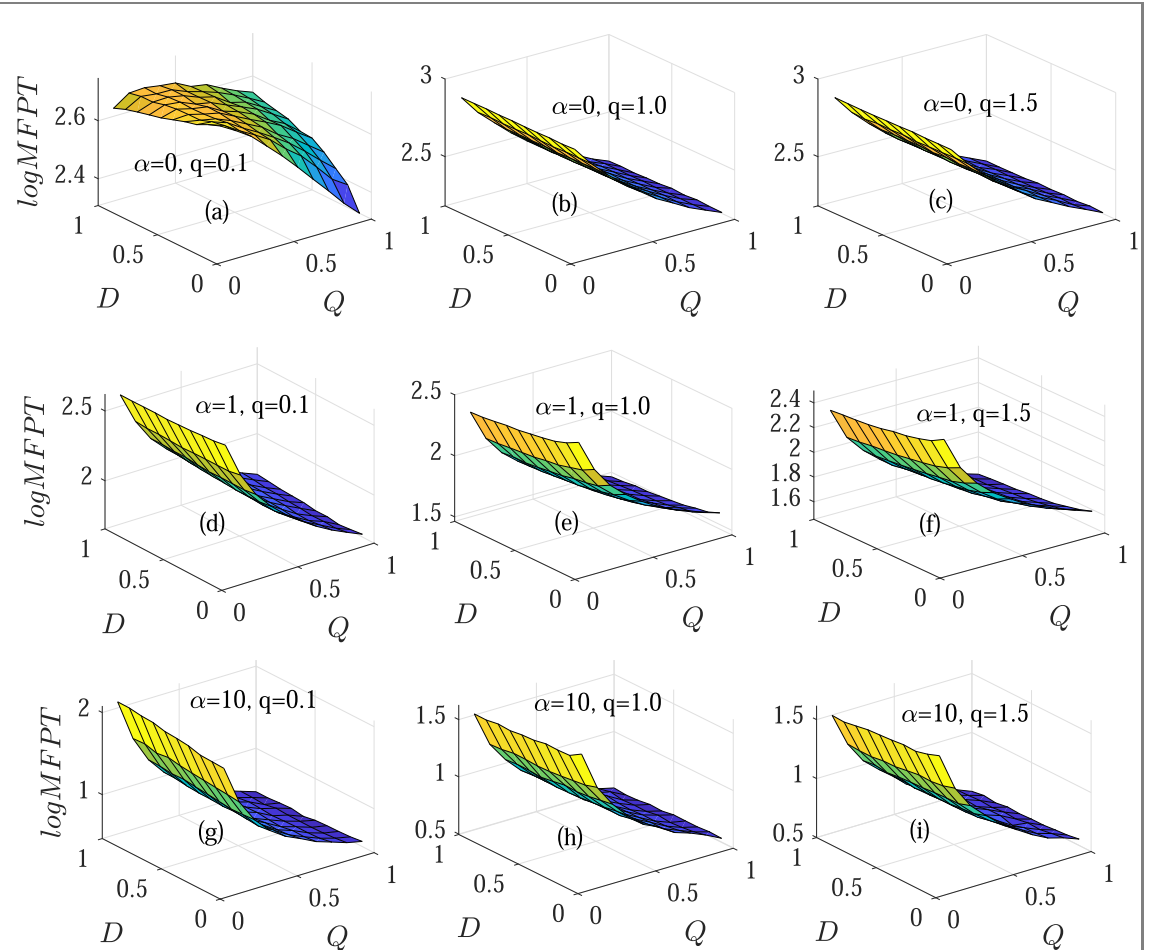


Figure 12. MFPT as function of the multiplicative non-Gaussian coloured noise intensity D and strength Q of the additive Gaussian white noise. The non-extensivity parameter q is varied horizontally as $q = 0.1, 1.0$, and 1.5 while the diffusivity scaling exponent α is varied vertically as $\alpha = 0, 1$, and 10 . In all panels we chose $D_0 = 0.01$, $\lambda = 1$, $\tau = 0.1$, and $M = 1 \times 10^4$. The initial position of the particles is at the origin.

Figure 13 shows the FPTD for different values of the non-extensivity parameter q and the noise–noise coupling strength λ ($\lambda = 0, 0.5$, and 1). The FPTDs exhibit long right tails and broaden with increasing λ . The PDFs are non-monotonic with peaks (maxima) at short times which indicates that short FPTs are more likely than long ones, but note that the MFPTs represented by the vertical lines are to the right of the peaks implying

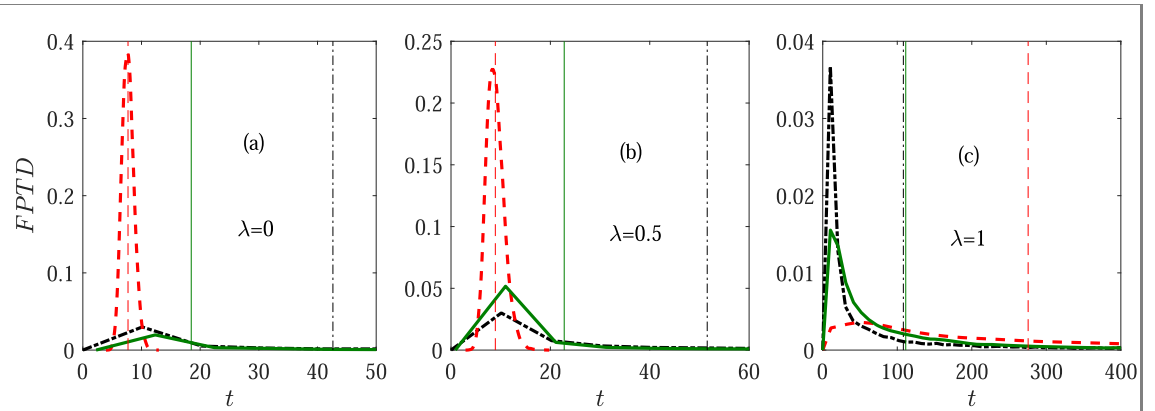


Figure 13. FPTD for different values of the non-extensivity parameter q ($q = 0.1$: black dash-dotted line; $q = 1$: red dashed line; $q = 1.5$: green solid line). The noise–noise coupling strength λ varies across the figure as $\lambda = 0, 0.5$, and 1 . In all panels we chose $D = 0.5$, $Q = 0.5$, $D_0 = 0.01$, $\tau = 0.1$, and $M = 1 \times 10^4$. The thin vertical lines in the corresponding line style and colours represent the respective MFPT. The initial position of the particles is at the origin.

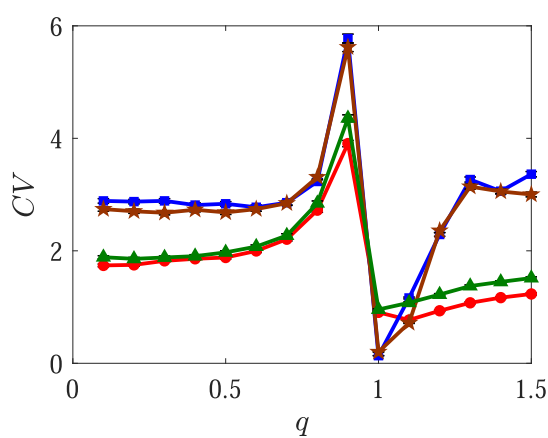


Figure 14. CV of the FPTD as function of the non-extensivity parameter q for different values of the noise–noise coupling strength λ . The solid lines with symbols represent the values $\lambda = -1$ (circles), $\lambda = 0$ (squares), $\lambda = 0.5$ (pentagrams), and $\lambda = 1$ (triangles). In all panels we chose $D = 0.5$, $Q = 0.5$, $D_0 = 0.01$, $\tau = 0.1$, and $M = 1 \times 10^4$. The initial position of the particles is at the origin. The error bars are of the order of the symbols.

that the long FPTs in the tail eventually dominate the MFPT. Thus, the FPT of a single trajectory may not be well represented by the MFPT.

Figure 14 shows the dependence of the CV of the FPTD on the non-extensivity parameter q . For all values of the noise–noise coupling strength λ the CV shows a similar shape: it first remains fairly constant and then increases rapidly to a maximum value at $q = 0.9$. It drops sharply to a minimum value at $q = 1$ and then increases with increasing q . Note that the curves for different λ actually show distinct crossings. Except for q close to one, the CV is greater than unity, implying high variation and broad distributions—in agreement with the observations of figure 13.

Figure 15 shows the MFPT as a function of the non-extensivity parameter q for different values of the noise–noise coupling strength λ . The MFPT increases with increasing $|\lambda|$, i.e., for a fixed small q , the MFPT is highest and lowest when $|\lambda| = 1$ and 0 , respectively. The MFPT shows a non-monotonic dependence on q , with an increase in q the MFPT first remains fairly constant, with gradual growth and descent for $\lambda = 0, 0.3, 0.5, 0.8$, and $|\lambda| = 1$ respectively, descends to a minimum value, before increasing to what appears like a plateau exhibiting a resonant activation-like phenomenon. The minimum value increases with increasing $|\lambda|$. Departure from Gaussianity leads to long MFPTs, i.e., it inhibits some particles from reaching the absorbing boundary. We also note that for $|\lambda| < 1$ the MFPT is long and short when $q < 1$ and $q > 1$, respectively. 95% confidence intervals for the MFPT under different values for q and λ are presented in table 3 appendix B.

Figure 16 presents the MFPT as function of the noise–noise correlation λ for different values of the non-extensivity parameter q . The minimum MFPT is realised when $\lambda = 0$. For all q values the MFPT increases with increasing $|\lambda|$. When λ is close to one and $q = 1.0$ the MFPT grows strongly with increasing λ . Generally, the MFPT is fairly symmetric about $\lambda = 0$. Both q and λ are relevant parameters for the variations of the MFPT.

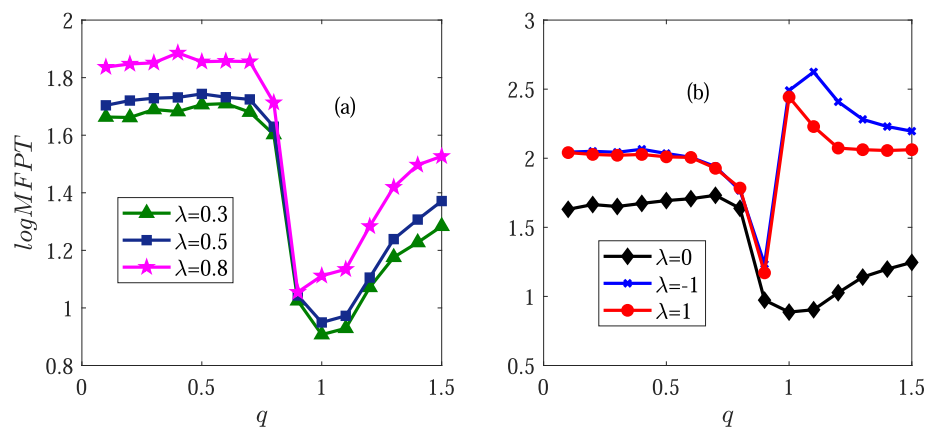


Figure 15. MFPT as function of the non-extensivity parameter q for different values of the noise–noise coupling strength λ . In all panels we chose $D = 0.5$, $Q = 0.5$, $D_0 = 0.01$, $\tau = 0.1$, and $M = 1 \times 10^4$. The initial position of the particles is at the origin.

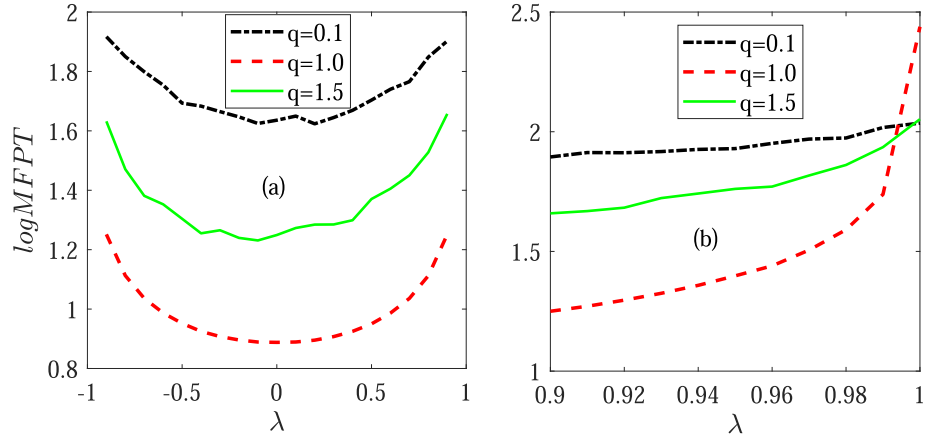


Figure 16. MFPT as a function of the noise–noise correlation strength λ for various values of the non-extensivity parameter q . We chose the parameters $D = 0.5$, $Q = 0.5$, $D_0 = 0.01$, $\tau = 0.1$, and $M = 1 \times 10^4$. The panel on the right shows a zoom into the region around $\lambda = 1.0$. The initial position is at the origin.

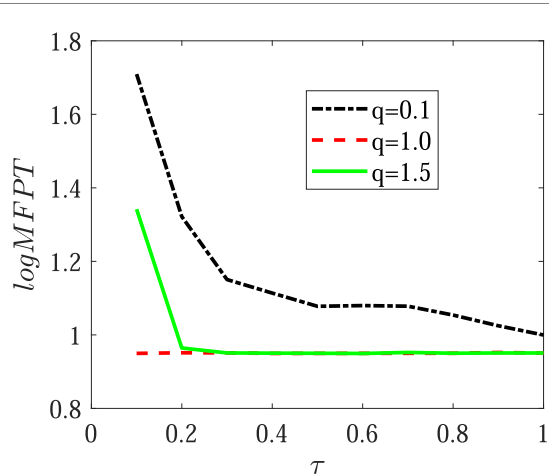


Figure 17. MFPT as function of the self-correlation time τ of the multiplicative coloured noise for various values of the non-extensivity parameter q . The parameters are chosen as $D = 0.5$, $Q = 0.5$, $D_0 = 0.01$, $\lambda = 0.5$, and $M = 1 \times 10^4$. The initial position of the particles is at the origin.

When $|\lambda|$ is close to one departure from Gaussianity leads to short MFPT, i.e., it accelerates particles reaching the boundary, otherwise departure from Gaussianity leads to long MFPT.

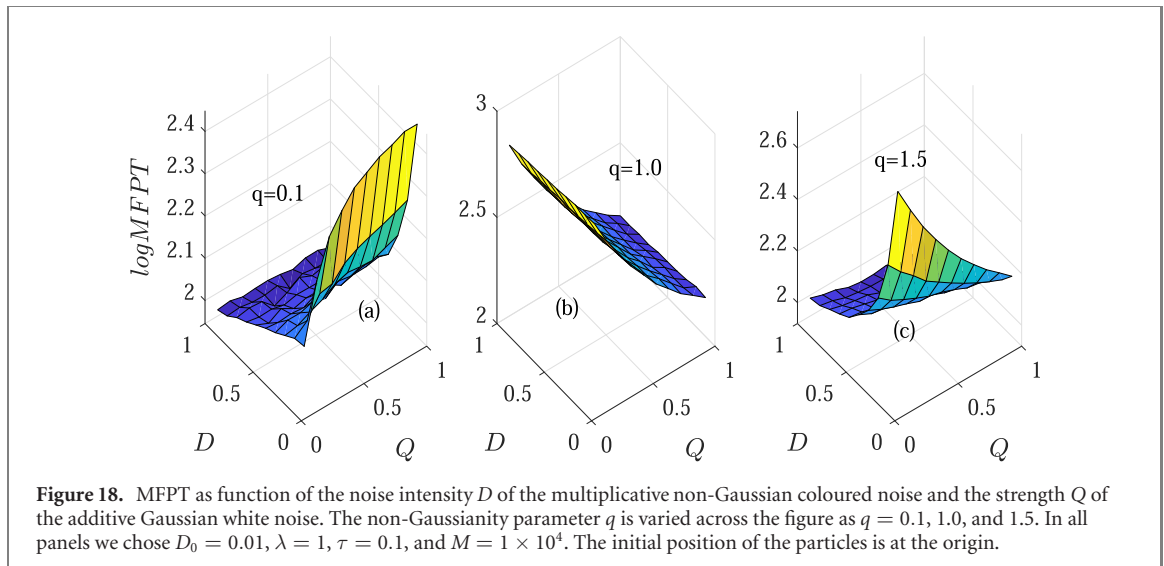


Figure 17 displays the dependence of the MFPT on the self-correlation time τ for different values of the non-extensivity parameter q . For $q = 1.0$ the MFPT remains constant over most of the τ range probed here, while for $q = 0.1$ and $q = 1.5$ it first decreases with increasing τ and then shows only smaller variations. We see that the non-Gaussianity ($q \neq 1$) impacts the MFPT mainly for small values of τ . For a fixed small τ non-Gaussianity leads to long MFPTs which arise from long FPT events.

Figure 18 presents the conspirative effect on the MFPT of the noise intensity D of the multiplicative non-Gaussian coloured noise and the strength Q of the additive Gaussian white noise, where q varies across the figure ($q = 0.1, 1.0, 1.5$). In panel (a) the MFPT decreases with increasing D but increases with growing Q . The MFPT is short when D is close to one. In the Gaussian case, panel (b), the MFPT decreases with increasing Q but remains fairly constant, with gradual descent, with variation of D . In panel (c) the MFPT first increases and then decreases with increase of both D and Q . The effect of D in accelerating particles to the absorbing boundary is more pronounced when the noise departs from Gaussian behaviour. Q changes its role, it accelerates particle to the absorbing boundary when $q > 1$ and inhibits particles when $q < 1$. We note that when $q > 1$, D and Q conspire to shorten the MFPT, while they act antagonistically when $q < 1$.

4. Conclusions

We numerically studied the FPT problem of stochastic motion in a one-dimensional heterogeneous system based on fourth-order Runge–Kutta simulations. The Langevin equation for this system involves the multiplicative position-dependent diffusion coefficient $D(x)$ for which we chose the Stratonovich interpretation. The process is driven by coloured non-Gaussian q -noise $\eta(t)$, whose dynamics is defined as an Ornstein–Uhlenbeck-type process with q -noise potential V_q and white Gaussian driving noise $\xi(t)$. The dynamic equation also contains an additive white Gaussian noise $\epsilon(t)$, that is coupled to the noise $\xi(t)$ via a noise–noise coupling of strength λ . For $D(x)$ we considered a power-law form as well as an exponential and logarithmic form. We studied in depth the FPT statistics as function of all model parameters. Specifically we observe clear crossover behaviours when the non-extensivity parameter q is close to the Gaussian value, $q = 1$, as well as $q = 0.9$. Especially for the CV of the FPTP we find values significantly exceeding unity, implying that the MFPT is in fact a bad estimate for the FPT-behaviour, matching recent findings on the full FPTD in even simple settings [10, 12, 34, 47]. Both departure from Gaussian behaviour of the multiplicative coloured noise and the noise–noise coupling lead to long FPT events. The MFPT as a function of the non-Gaussian parameter q and the correlation time τ of the coloured noise exhibits resonant activation-like phenomena. Also, depending on q the parameters D and Q can collaborate or act on particle in the opposite directions. The wealth of the dynamics encoded in this generalised heterogeneous diffusion process is a versatile starting point for the analysis of stochastic dynamics in complex, heterogeneous systems and non-Markovian dynamics. The model reported here particularly allows the study of tradeoff effects between the non-Gaussianity, correlations in the noise, and the noise–noise coupling, with respect to the inhomogeneity of the diffusion coefficient.

In future work it will be of interest to modify the deterministic dependence of the diffusion coefficient $D(x)$ for patchy diffusivity distributions in both the annealed and quenched limits, to more closely mimic diffusion and first-passage in disordered systems. While such an extension will require numerical simulations to obtain

the associated statistics, the results reported here will be useful as a benchmark for specific systems governed by different types of noises. It would also be interesting to include switching types of potentials [154] and consider explicit environmental noise, e.g., in population dynamics and competition [58, 155]. Another possible line of generalisation is to include a time dependence of the diffusion coefficient and study how this affects the first passage behaviour.

Acknowledgments

RM acknowledges the Foundation for Polish Science (Fundacja na rzecz Nauki Polskiej, FNP) for support within an Alexander von Humboldt Polish Honorary Research Scholarship as well as the German Science Foundation (DFG Grant ME 1535/12-1). This paper was supported by the National Natural Science Foundation of China under Grant Nos. 12072264 and 11902118, the Key International (Regional) Joint Research Program of NSF of China under Grant No. 12120101002, the Research Funds for Interdisciplinary Subject of Northwestern Polytechnical University, Shaanxi Provincial Key R & D Program 2020KW-013 and 2019TD-010, and the Foundation of Key Laboratory of Structural Mechanics and Intelligent Materials of Hebei Province.

Data availability statement

No new data were created or analysed in this study.

Appendix A. Numerical discretisation scheme

Here we use a discrete representation based on the fourth-order Runge–Kutta-type integration scheme to simulate the particle trajectories and record the FPT. We first rewrite the stochastic equations (1) and (2) in the form

$$\frac{dx(t)}{dt} = f(x(t), \eta(t)), \quad (A1)$$

$$\frac{d\eta(t)}{dt} = h(\eta(t), q) + \frac{1}{\tau}\xi(t), \quad (A2)$$

where $f(x(t), \eta(t)) = \sqrt{2D(x(t))} \times \eta(t)$ and $h(\eta, q) = -\frac{1}{\tau} \left[\frac{2\eta(t)}{2+\eta(t)^2(q-1)\beta} \right]$. We generate sets of standard normal random variables $Z_{1k} = \{z_{1k}(i)\}$ and $Z_{2k} = \{z_{2k}(i)\}$ where $k = 0, 1, 2, 3, 4$. $z_{1k}(i)$ and $z_{2k}(i)$ are normally distributed random variables with zero mean and unit variance. We then compute

$$R_k(i) = \sqrt{2D\Delta t} \times z_{1k}(i),$$

$$S_k(i) = \sqrt{2Q\Delta t} \left(\lambda z_{1k}(i) + \sqrt{1-\lambda^2} z_{2k(i)} \right).$$

Then, the numerical iteration scheme reads

$$x(i+1) = x(i) + \frac{\Delta t}{6} \times [F_1(i) + 2F_2(i) + 2F_3(i) + F_4(i)] + S_0(i), \quad (A3)$$

$$\eta(i+1) = \eta(i) + \frac{\Delta t}{6} \times [H_1(i) + 2H_2(i) + 2H_3(i) + H_4(i)] + \frac{R_0(i)}{\tau}, \quad (A4)$$

where

$$F_1(i) = \sqrt{2D[x(i) + S_1(i)]} \times (\eta(i) + R_1(i)/\tau) \quad (A5)$$

$$F_2(i) = \sqrt{2 \left\{ D \left[x(i) + \frac{\Delta t}{2} \times F_1(i) + S_2(i) \right] \right\}}$$

$$\times \left(\eta(i) + \frac{\Delta t}{2} \times H_1(i) + \frac{R_2(i)}{\tau} \right) \quad (A6)$$

$$F_3(i) = \sqrt{2 \left\{ D \left[x(i) + \frac{\Delta t}{2} \times F_2(i) + S_3(i) \right] \right\}}$$

$$\times \left(\eta(i) + \frac{\Delta t}{2} \times H_2(i) + \frac{R_3(i)}{\tau} \right) \quad (A7)$$

Table 1. 95% confidence interval for the MFPT when function form for the coefficient is the power-law (4).

q	$\lambda = 0$			$\lambda = 0.5$			$\lambda = 1.0$		
	$\alpha = -1$	$\alpha = 0$	$\alpha = 1$	$\alpha = -1$	$\alpha = 0$	$\alpha = 1$	$\alpha = -1$	$\alpha = 0$	$\alpha = 1$
0.1	58 ± 9	53 ± 9	47 ± 8	60 ± 9	54 ± 9	48 ± 8	68 ± 10	59 ± 9	50 ± 9
0.2	59 ± 9	54 ± 9	48 ± 8	61 ± 9	55 ± 9	48 ± 8	69 ± 10	59 ± 9	52 ± 9
0.3	59 ± 9	55 ± 9	49 ± 9	61 ± 9	55 ± 9	50 ± 9	70 ± 10	59 ± 9	53 ± 9
0.4	60 ± 9	55 ± 9	50 ± 9	62 ± 10	56 ± 9	51 ± 9	69 ± 10	60 ± 10	54 ± 9
0.5	60 ± 10	55 ± 9	52 ± 9	62 ± 10	58 ± 9	51 ± 9	68 ± 10	61 ± 10	54 ± 9
0.6	60 ± 10	54 ± 9	51 ± 9	61 ± 10	55 ± 9	52 ± 9	66 ± 10	58 ± 10	52 ± 9
0.7	54 ± 9	50 ± 9	47 ± 9	56 ± 10	51 ± 9	48 ± 9	58 ± 10	52 ± 9	49 ± 9
0.8	34 ± 7	32 ± 7	31 ± 7	36 ± 8	33 ± 7	31 ± 7	37 ± 8	33 ± 7	31 ± 7
0.9	4 ± 2	4 ± 2	3 ± 2	4 ± 2	3 ± 2	3 ± 2	5 ± 2	4 ± 2	3 ± 2
1.0	7.8 ± 0.1	7.7 ± 0.1	7.7 ± 0.1	9.4 ± 0.2	9.1 ± 0.2	8.5 ± 0.2	210 ± 13	153 ± 10	93 ± 6
1.1	10 ± 1	10 ± 1	8 ± 1	12 ± 1	12 ± 1	9 ± 1	58 ± 4	34 ± 2	21 ± 2
1.2	15 ± 2	15 ± 2	12 ± 2	18 ± 2	16 ± 2	12 ± 2	44 ± 4	28 ± 3	19 ± 3
1.3	21 ± 3	20 ± 3	16 ± 3	24 ± 4	21 ± 4	16 ± 3	46 ± 5	31 ± 4	22 ± 4
1.4	26 ± 4	23 ± 4	19 ± 4	29 ± 5	25 ± 4	20 ± 4	48 ± 6	34 ± 5	25 ± 4
1.5	29 ± 5	27 ± 5	28 ± 5	32 ± 5	28 ± 5	22 ± 4	51 ± 7	37 ± 6	28 ± 5

Table 2. 95% confidence interval for the MFPT when function form for the diffusion coefficient is the exponential (5).

q	$\lambda = 0$			$\lambda = 0.5$			$\lambda = 1.0$		
	$\alpha = 0$	$\alpha = 1$	$\alpha = 10$	$\alpha = 0$	$\alpha = 1$	$\alpha = 10$	$\alpha = 0$	$\alpha = 1$	$\alpha = 10$
0.1	39 ± 8	9 ± 2	9 ± 1	53 ± 9	16 ± 3	19 ± 4	114 ± 13	121 ± 11	49 ± 8
0.2	40 ± 8	9 ± 2	9 ± 1	54 ± 9	17 ± 4	19 ± 4	113 ± 14	121 ± 11	51 ± 8
0.3	42 ± 8	9 ± 2	9 ± 1	55 ± 3	17 ± 4	20 ± 4	113 ± 14	122 ± 11	53 ± 8
0.4	43 ± 8	10 ± 2	9 ± 1	57 ± 10	17 ± 4	21 ± 4	111 ± 14	124 ± 11	56 ± 9
0.5	45 ± 9	10 ± 2	9 ± 1	59 ± 10	17 ± 4	22 ± 5	111 ± 14	125 ± 11	58 ± 9
0.6	46 ± 9	10 ± 2	9 ± 2	60 ± 10	17 ± 4	22 ± 5	107 ± 14	122 ± 11	59 ± 9
0.7	47 ± 9	9 ± 2	9 ± 1	59 ± 11	17 ± 4	23 ± 5	97 ± 14	119 ± 11	57 ± 9
0.8	41 ± 9	9 ± 1	9 ± 1	49 ± 10	14 ± 3	19 ± 4	74 ± 13	102 ± 9	49 ± 8
0.9	13 ± 5	7.8 ± 0.3	7.8 ± 0.3	15 ± 6	9 ± 1	9 ± 1	23 ± 7	74 ± 4	25 ± 3
1.0	7.7 ± 0.1	7.7 ± 0.1	7.7 ± 0.1	8.9 ± 0.1	9.3 ± 0.8	8.6 ± 0.2	279 ± 17	40 ± 2	6 ± 1
1.1	8 ± 0.3	7.7 ± 0.1	7.7 ± 0.1	9.5 ± 0.5	9 ± 0.2	8.1 ± 0.2	174 ± 11	35 ± 2	7 ± 1
1.2	10 ± 1	7.7 ± 0.1	7.7 ± 0.1	13 ± 2	9 ± 1	9 ± 1	123 ± 9	43 ± 4	10 ± 2
1.3	12 ± 2	7.7 ± 0.1	7.7 ± 0.1	17 ± 3	10 ± 1	9 ± 1	115 ± 10	54 ± 5	13 ± 3
1.4	15 ± 3	7.7 ± 0.1	7.7 ± 0.2	21 ± 4	10 ± 1	10 ± 1	115 ± 11	62 ± 6	15 ± 3
1.5	16 ± 3	7.7 ± 0.1	7.7 ± 0.2	23 ± 4	11 ± 1	10 ± 2	114 ± 11	69 ± 7	17 ± 4

$$F_4(i) = \sqrt{2 \left\{ D \left[x(i) + \frac{\Delta t}{2} \times F_3(i) + S_4(i) \right] \right\}} \\ \times \left(\eta(i) + \frac{\Delta t}{2} \times H_3(i) + \frac{R_4(i)}{\tau} \right) \quad (\text{A8})$$

$$H_1(i) = -\frac{2(\eta(i) + R_1/\tau)/\tau}{2 + (\eta(i) + R_1/\tau)^2 \times (q-1) \times \beta} \quad (\text{A9})$$

$$H_2(i) = -\frac{2 \left[\eta(i) + \frac{\Delta t}{2} \times H_1(i) + \frac{R_2(i)}{\tau} \right] / \tau}{2 + \left[\eta(i) + \frac{\Delta t}{2} \times H_1(i) + \frac{R_2(i)}{\tau} \right]^2 \times (q-1) \times \beta} \quad (\text{A10})$$

$$H_3(i) = -\frac{2 \left[\eta(i) + \frac{\Delta t}{2} \times H_2(i) + \frac{R_3(i)}{\tau} \right] / \tau}{2 + \left[\eta(i) + \frac{\Delta t}{2} \times H_2(i) + \frac{R_3(i)}{\tau} \right]^2 \times (q-1) \times \beta} \quad (\text{A11})$$

$$H_4(i) = -\frac{2 \left[\eta(i) + \frac{\Delta t}{2} \times H_3(i) + \frac{R_4(i)}{\tau} \right] / \tau}{2 + \left[\eta(i) + \frac{\Delta t}{2} \times H_3(i) + \frac{R_4(i)}{\tau} \right]^2 \times (q-1) \times \beta}, \quad (\text{A12})$$

for $i = 1, 2, \dots$

Appendix B. 95% confidence interval for the MFPT

The tables in this appendix present 95% confidence intervals for the MFPT. The specific values of the non-Gaussianity parameter q , the diffusivity scaling exponent α , and the noise–noise coupling strength λ are indicated in the tables. Other parameters are fixed: $D = 0.5$, $Q = 0.5$, $D_0 = 0.01$, and $\tau = 0.1$. To determine the confidence interval we first simulated 10 samples each of 1×10^4 FPT observations, calculated pooled mean and standard deviation, and then determined the confidence interval.

Table 3. 95% confidence interval for the MFPT when function form for the coefficient has the logarithmic expression (6).

q	$\lambda = 0$	$\lambda = 0.3$	$\lambda = 0.5$	$\lambda = 0.8$	$\lambda = -1$	$\lambda = 1$
0.1	43 ± 8	45 ± 8	50 ± 9	70 ± 10	115 ± 13	108 ± 13
0.2	44 ± 8	48 ± 8	52 ± 9	69 ± 10	112 ± 13	109 ± 13
0.3	45 ± 8	47 ± 8	53 ± 9	72 ± 11	112 ± 13	106 ± 13
0.4	47 ± 8	50 ± 9	55 ± 9	72 ± 11	109 ± 13	106 ± 13
0.5	49 ± 9	50 ± 9	55 ± 9	74 ± 11	106 ± 13	101 ± 13
0.6	52 ± 9	52 ± 9	57 ± 10	73 ± 11	99 ± 13	97 ± 13
0.7	52 ± 9	51 ± 9	55 ± 10	68 ± 11	87 ± 12	87 ± 12
0.8	44 ± 9	42 ± 8	43 ± 9	50 ± 10	60 ± 10	58 ± 10
0.9	10 ± 3	11 ± 4	10 ± 4	12 ± 5	17 ± 4	16 ± 5
1.0	7.7 ± 0.1	8.1 ± 0.1	8.9 ± 0.1	12.9 ± 0.3	310 ± 18	278 ± 17
1.1	8 ± 0.3	8.5 ± 0.4	9.3 ± 0.4	14 ± 1	426 ± 21	173 ± 12
1.2	10 ± 2	11 ± 2	13 ± 2	19 ± 2	256 ± 15	121 ± 9
1.3	13 ± 2	15 ± 3	17 ± 3	25 ± 4	189 ± 13	114 ± 10
1.4	16 ± 3	17 ± 3	20 ± 4	30 ± 5	168 ± 13	113 ± 10
1.5	18 ± 3	19 ± 4	23 ± 4	34 ± 5	158 ± 12	113 ± 11

ORCID iDs

Yong Xu  <https://orcid.org/0000-0002-8407-4650>

Ralf Metzler  <https://orcid.org/0000-0002-6013-7020>

References

- [1] Barkai E, Garini Y and Metzler R 2012 Strange kinetics of single molecules in living cells *Phys. Today* **65** 29
- [2] Caspi A, Granek R and Elbaum M 2000 Enhanced diffusion in active intracellular transport *Phys. Rev. Lett.* **85** 5655
- [3] Reverey J F, Jeon J-H, Bao H, Leippe M, Metzler R and Selhuber-Unkel C 2015 Superdiffusion dominates intracellular particle motion in the supercrowded cytoplasm of pathogenic *Acanthamoeba castellanii* *Sci. Rep.* **5** 11690
- [4] Seisenberger G, Ried M U, Endreß T, Büning H, Hallek M and Bräuchle C 2001 Real-time single-molecule imaging of the infection pathway of an adeno-associated virus *Science* **294** 1929
- [5] Di Renzo C, Piazza V, Gratton E, Beltram F and Cardarelli F 2014 Probing short-range protein Brownian motion in the cytoplasm of living cells *Nat. Commun.* **5** 5891
- [6] Kühn T, Ihlainen T O, Hyväloma J, Dross N, Willman S F, Langowski J, Vihtinen-Ranta M and Timonen J 2011 Protein diffusion in mammalian cell cytoplasm *PLoS One* **6** e22962
- [7] Kuhlman T E and Cox E C 2012 Gene location and DNA density determine transcription factor distributions in *Escherichia coli* *Mol. Syst. Biol.* **8** 610
- [8] Képès F 2004 Periodic transcriptional organization of the *E. coli* genome *J. Mol. Biol.* **340** 957
- [9] Kolesov G, Wunderlich Z, Laikova O N, Gelfand M S and Mirny L A 2007 How gene order is influenced by the biophysics of transcription regulation *Proc. Natl Acad. Sci. USA* **104** 13948
- [10] Grebenkov D S, Metzler R and Oshanin G 2018 Strong defocusing of molecular reaction times results from an interplay of geometry and reaction control *Commun. Chem.* **1** 96
- [11] Pulkkinen O and Metzler R 2013 Distance matters: the impact of gene proximity in bacterial gene regulation *Phys. Rev. Lett.* **110** 198101
- [12] Godec A and Metzler R 2016 Universal proximity effect in target search kinetics in the few encounter limit *Phys. Rev. X* **6** 041037
- [13] Smoluchowski M v 1917 Versuch einer mathematischen Theorie der Koagulationskinetik kolloider Lösungen *Z. Phys. Chem.* **92** 129
- [14] Collins F C and Kimball G E 1949 Diffusion-controlled reaction rates *J. Colloid Sci.* **4** 425
- [15] Redner S 2001 *A Guide to First Passage Processes* (Cambridge: Cambridge University Press)
- [16] Metzler R, Oshanin G and Redner S 2014 *First-Passage Phenomena and Their Applications* (Singapore: World Scientific)
- [17] Pizzolato N, Fiasconaro A, Adorno D P and Spagnolo B 2010 *Phys. Biol.* **7** 034001
- [18] Viswanathan G M, da Luz M G E, Raposo E P and Stanley H E 2011 *The Physics of Foraging* (Cambridge: Cambridge University Press)
- [19] Hufnagel L, Brockmann D and Geisel T 2004 Forecast and control of epidemics in a globalized world *Proc. Natl Acad. Sci. USA* **101** 15124

- [20] Gross B, Zheng Z, Liu S, Chen X, Sela A, Li J, Li D and Havlin S 2020 Spatio-temporal propagation of COVID-19 pandemics *Europhys. Lett.* **131** 58003
- [21] Valenti D, Fazio G and Spagnolo B 2018 Stabilizing effect of volatility in financial markets *Phys. Rev. E* **97** 062307
- [22] Spagnolo B and Valenti D 2008 Volatility effects on the escape time in financial market models *Int. J. Bifurcation Chaos* **18** 2775
- [23] Goepfert N, Goldscheider N and Berkowitz B 2020 Experimental and modeling evidence of kilometer-scale anomalous tracer transport in an alpine karst aquifer *Water Res.* **178** 115755
- [24] Bouchaud J-P and Potters M 2000 *Theory of Financial Risk and Derivative Pricing: From Statistical Physics to Risk Management* (Cambridge: Cambridge University Press)
- [25] Bénichou O, Coppey M, Moreau M, Suet P-H and Voituriez R 2005 Optimal search strategies for hidden targets *Phys. Rev. Lett.* **94** 198101
- [26] Mckenzie H W, Lewis M A and Merrill E H 2008 First passage time analysis of animal movement and insights into the functional response *Bull. Math. Biol.* **71** 107
- [27] Tejedor V, Bénichou O and Voituriez R 2009 Global mean first-passage times of random walks on complex networks *Phys. Rev. E* **80** 065104(R)
- [28] Hartich D and Godec A 2019 Extreme value statistics of ergodic Markov processes from first passage times in the large deviation limit *J. Phys. A: Math. Theor.* **52** 244001
- [29] Bray A J, Majumdar S N and Schehr G 2013 Persistence and first-passage properties in nonequilibrium systems *Adv. Phys.* **62** 225
- [30] Johnson A R, Wiens J A, Milne B T and Crist T O 1992 Animal movements and population dynamics in heterogeneous landscapes *Landsc. Ecol.* **7** 63
- [31] Condamin S, Tejedor V, Voituriez R, Bénichou O and Klafter J 2007 Probing microscopic origins of confined subdiffusion by first-passage observables *Proc. Natl Acad. Sci. USA* **105** 5675
- [32] Jeon J-H, Monne H M-S, Javanainen M and Metzler R 2012 Anomalous diffusion of phospholipids and cholesterols in a lipid bilayer and its origins *Phys. Rev. Lett.* **109** 188103
- [33] Lawley S D 2020 Universal formula for extreme first passage statistics of diffusion *Phys. Rev. E* **101** 012413
- [34] Grebenkov D S, Metzler R and Oshanin G 2020 From single-particle stochastic kinetics to macroscopic reaction rates: fastest first-passage time of N random walkers *New J. Phys.* **22** 103004
- [35] Schuss Z, Basnayake K and Holcman D 2019 Redundancy principle and the role of extreme statistics in molecular and cellular biology *Phys. Life Rev.* **28** 52
- [36] Weiss G H, Shuler K E and Lindenberg K 1983 Order statistics for first passage times in diffusion processes *J. Stat. Phys.* **31** 255
- [37] Meerson B and Redner S 2015 Mortality, redundancy, and diversity in stochastic search *Phys. Rev. Lett.* **114** 198101
- [38] Condamin S, Bénichou O, Tejedor V, Voituriez R and Klafter J 2007 First-passage times in complex scale-invariant media *Nature* **450** 77
- [39] Lindsay A E, Bernoff A J and Ward M J 2017 First passage statistics for the capture of a Brownian particle by a structured spherical target with multiple surface traps *Multiscale Model. Simul.* **15** 74
- [40] Lou X, Guo Y, Dong Q and Wei Y 2020 First-passage behavior of periodic potential system driven by correlated noise *Chin. J. Phys.* **68** 270
- [41] Jin Y 2012 Noise-induced dynamics in a delayed bistable system with correlated noises *Physica A* **391** 1909
- [42] Li H, Xu Y, Yue X and Kurths J 2019 Transition-event duration in one-dimensional systems under correlated noise *Physica A* **532** 121764
- [43] Mutothya N M and Xu Y 2020 Mean first passage time for diffuse and rest search in a confined spherical domain *Physica A* **567** 125667
- [44] Li Y, Xu Y and Kurths J 2019 First-passage-time distribution in a moving parabolic potential with spatial roughness *Phys. Rev. E* **99** 052203
- [45] Lawley S D and Miles C E 2019 Diffusive search for diffusing targets with fluctuating diffusivity and gating *J. Nonlinear Sci.* **29** 2955
- [46] Godec A and Metzler R 2017 First passage time statistics for two-channel diffusion *J. Phys. A: Math. Theor.* **50** 084001
- [47] Godec A and Metzler R 2016 First passage time distribution in heterogeneity controlled kinetics: going beyond the mean first passage time *Sci. Rep.* **6** 20349
- [48] Weber S C, Spakowitz A J and Theriot J A 2010 Bacterial chromosomal loci move subdiffusively through a viscoelastic cytoplasm *Phys. Rev. Lett.* **104** 238102
- [49] Weigel A V, Simon B, Tamkun M M and Krapf D 2011 Ergodic and nonergodic processes coexist in the plasma membrane as observed by single-molecule tracking *Proc. Natl Acad. Sci. USA* **108** 6438
- [50] Tabei S M A, Burov S, Kim H Y, Kuznetsov A, Huynh T, Jureller J, Philipson L H, Dinner A R and Scherer N F 2013 Intracellular transport of insulin granules is a subordinated random walk *Proc. Natl Acad. Sci. USA* **110** 4911
- [51] Jeon J-H, Javanainen M, Martinez-Seara H, Metzler R and Vattulainen I 2016 Protein crowding in lipid bilayers gives rise to non-Gaussian anomalous lateral diffusion of phospholipids and proteins *Phys. Rev. X* **6** 021006
- [52] Lampo T J, Stylianidou S, Backlund M P, Wiggins P A and Spakowitz A J 2017 Cytoplasmic RNA-protein particles exhibit non-Gaussian subdiffusive behavior *Biophys. J.* **112** 532
- [53] Marini U, Marconi B and Puglisi A 2002 Mean-field model of free-cooling inelastic mixtures *Phys. Rev. E* **65** 051305
- [54] Scher H and Montroll E W 1975 Anomalous transit-time dispersion in amorphous solids *Phys. Rev. B* **12** 2455
- [55] Jeon J-H, Leijnse N, Oddershede L B and Metzler R 2013 Anomalous diffusion and power-law relaxation of the time averaged mean squared displacement in worm-like micellar solutions *New J. Phys.* **15** 045011
- [56] Mutothya N M, Xu Y, Li Y and Metzler R 2021 Characterising stochastic motion in heterogeneous media driven by coloured non-Gaussian noise *J. Phys. A: Math. Theor.* **54** 295002
- [57] Xu Y, Liu X, Li Y and Metzler R 2020 Heterogeneous diffusion processes and non-ergodicity with Gaussian coloured noise in layered diffusivity landscapes *Phys. Rev. E* **102** 062106
- [58] Denaro G et al 2013 Spatio-temporal behaviour of the deep chlorophyll maximum in Mediterranean Sea: development of a stochastic model for picophytoplankton dynamics *Ecol. Complex.* **13** 21
- [59] Cherstvy A G, Chechkin A V and Metzler R 2013 Anomalous diffusion and ergodicity breaking in heterogeneous diffusion processes *New J. Phys.* **15** 083039
- [60] Volpe G and Wehr J 2016 Effective drifts in dynamical systems with multiplicative noise: a review of recent progress *Rep. Prog. Phys.* **79** 053901

- [61] Castro F J, Kuperman N M, Fuentes M and Wio H S 2001 Experimental evidence of stochastic resonance without tuning due to non Gaussian noises *Phys. Rev. E* **64** 051105
- [62] Fuentes M A, Wio H S and Toral R 2002 Effective Markovian approximation for non-Gaussian noises: a path integral approach *Physica A* **303** 91
- [63] Hänggi P and Jung P 1995 Colored noise in dynamical systems *Adv. Chem. Phys.* **89** 239
- [64] Jung P and Hänggi P 1987 Dynamical systems: a unified colored-noise approximation *Phys. Rev. A* **35** 4464(R)
- [65] Hasegawa H 2007 A moment approach to non-Gaussian colored noise *Physica A* **384** 241
- [66] Wio H S 2004 On the role of non-Gaussian noises on noise-induced Phenomena *Nonextensive Entropy* ed M Gell-Mann and C Tsallis (Oxford: Oxford University Press)
- [67] Wio H S 2005 Noise induced phenomena and nonextensivity *Europhys. News* **36** 197
- [68] Deza J I and Deza R R 2018 *qNoise*: a generator of non-Gaussian colored noise (arXiv:1812.07451)
- [69] Wang K-K, Zong D-C, Zhou Y and Wu J-C 2016 Stochastic dynamical features for a time-delayed ecological system of vegetation subjected to correlated multiplicative and additive noises *Chaos Solitons Fractals* **91** 490
- [70] Yang Y-F, Wang C-J, Yang K-L, Yang Y-Q and Zheng Y-C 2019 Impacts of the cross-correlated noises on the fluctuation behaviors of a gene transcriptional regulatory system *Physica A* **514** 580
- [71] Bag B C and Hu C K 2006 Escape through an unstable limit cycle: resonant activation *Phys. Rev. E* **73** 061107
- [72] Bag B C and Hu C K 2007 Escape through an unstable limit cycle driven by multiplicative colored non-Gaussian and additive white Gaussian noises *Phys. Rev. E* **75** 042101
- [73] Shi P, Su X, Han D, Fu R and Ma X 2017 The stable state properties and mean first-passage time of tristable system driven by non-correlated additive and multiplicative non-Gaussian noise *Chin. J. Phys.* **55** 2124
- [74] Jin Y and Xu W 2005 Mean first-passage time of a bistable kinetic model driven by two different kinds of coloured noises *Chaos Solitons Fractals* **23** 275
- [75] Xie C W and Mei D C 2003 Mean first-passage time of a bistable kinetic model driven by multiplicative coloured noise and additive white noise *Chin. Phys. Lett.* **20** 813
- [76] Li Y, Xu Y, Kurths J and Yue X 2017 Transports in a rough ratchet induced by Lévy noises *Chaos* **27** 103102
- [77] Zan W, Xu Y, Metzler R and Kurths J 2021 First-passage problem for stochastic differential equations with combined parametric Gaussian and Lévy white noises via path integral method *J. Comput. Phys.* **435** 110264
- [78] Wang Z, Xu Y and Yang H 2016 Lévy noise induced stochastic resonance in an FHN model *Sci. China Technol. Sci.* **59** 371
- [79] Guarcello C, Valenti D, Carollo A and Spagnolo B 2016 *J. Stat. Mech.* **054012**
- [80] Dubkov A A, La Cognata A and Spagnolo B 2009 *J. Stat. Mech.* **P01002**
- [81] Goswami G, Majee P, Kumar Ghosh P and Bag B C 2007 Colored multiplicative and additive non-Gaussian noise-driven dynamical system: mean first passage time *Physica A* **374** 549
- [82] Guo Y-F, Xi B, Wei F and Tan J-G 2018 The mean first-passage time in simplified FitzHugh–Nagumo neural model driven by correlated non-Gaussian noise and Gaussian noise *Mod. Phys. Lett. B* **32** 1850339
- [83] van Hijkkoop V J, Dammers A J, Malek K and Coppens M-O 2007 Water diffusion through a membrane protein channel: a first passage time approach *J. Chem. Phys.* **127** 085101
- [84] Bressloff P C and Lawley S D 2017 Residence times of a Brownian particle with temporal heterogeneity *J. Phys. A: Math. Theor.* **50** 195001
- [85] Bressloff P C and Lawley S D 2017 Temporal disorder as a mechanism for spatially heterogeneous diffusion *Phys. Rev. E* **95** 060101
- [86] Lanoiselle Y, Moutal N and Grebenkov D S 2018 Diffusion-limited reactions in dynamic heterogeneous media *Nat. Commun.* **9** 4398
- [87] Vaccario G, Antoine C and Talbot J 2015 First-passage times in d -dimensional heterogeneous media *Phys. Rev. Lett.* **115** 240601
- [88] Grebenkov D G and Tupikina L 2018 Heterogeneous continuous-time random walks *Phys. Rev. E* **97** 012148
- [89] Jung P and Hänggi P 1988 Bistability and colored noise in nonequilibrium systems: theory versus precise numerics *Phys. Rev. Lett.* **61** 11
- [90] Bray A J and McKane A J 1989 Instanton calculation of the escape rate for activation over a potential barrier driven by colored noise *Phys. Rev. Lett.* **62** 493
- [91] Leiber T, Marchesoni F and Risken H 1987 Colored noise and bistable Fokker–Planck equations *Phys. Rev. Lett.* **59** 1381
- [92] Dixit S N and Sahni P S 1983 Nonlinear stochastic processes driven by colored noise: application to dye-laser statistics *Phys. Rev. Lett.* **50** 1273
- [93] Lett P, Short R and Mandel L 1984 Photon statistics of a dye laser far below threshold *Phys. Rev. Lett.* **52** 341
- [94] Zhu S, Yu A W and Roy R 1986 Statistical fluctuations in laser transients *Phys. Rev. A* **34** 4333
- [95] Kubo R 1962 *Fluctuations, Relaxation and Resonance in Magnetic Systems* ed D ter Haar (Edinburgh: Edinburgh University Press)
- [96] Spanio T, Hidalgo J and Muñoz M A 2017 Impact of environmental colored noise in single-species population dynamics *Phys. Rev. E* **96** 042301
- [97] Müller-Hansen F, Droste F and Lindner B 2015 Statistics of a neuron model driven by asymmetric colored noise *Phys. Rev. E* **91** 022718
- [98] Mei R, Xu Y, Li Y and Kurths J 2020 The steady current analysis in a periodic channel driven by correlated noises *Chaos Solitons Fractals* **135** 109766
- [99] Zhang X, Xu Y, Liu Q and Kurths J 2020 Rate-dependent tipping-delay phenomenon in a thermoacoustic system with colored noise *Sci. China Technol. Sci.* **63** 2316
- [100] Lehle B and Peinke J 2018 Analyzing a stochastic process driven by Ornstein–Uhlenbeck noise *Phys. Rev. E* **97** 012113
- [101] Mandelbrot B B and van Ness J W 1968 Fractional Brownian motions, fractional noises and applications *SIAM Rev.* **10** 422
- [102] Qian H 2003 Fractional Brownian motion and fractional Gaussian noise *Processes with Long-Range Correlations: Theory and Applications* ed G Rangarajan and M Z Ding (Berlin: Springer)
- [103] Molina-Garcia D, Sandev T, Safdari H, Pagnini G, Chechkin A and Metzler R 2018 Crossover from anomalous to normal diffusion: truncated power-law noise correlations and applications to dynamics in lipid bilayers *New J. Phys.* **20** 103027
- [104] Meerschaert M M and Sabzikar F 2013 Tempered fractional Brownian motion *Stat. Probab. Lett.* **83** 2269
- [105] Picolo S, Mendes R S, Malacarne L C and Santos R P B 2009 *q*-distributions in complex systems: a brief review *Braz. J. Phys.* **39** 468
- [106] Budini A 2015 Extended *q*-Gaussian and *q*-exponential distributions from gamma random variables *Phys. Rev. E* **91** 052113

- [107] Tsallis C 1988 Possible generalization of Boltzmann–Gibbs statistics *J. Stat. Phys.* **52** 479
- [108] Tsallis C 2009 *Introduction to Nonextensive Statistical Mechanics* (New York: Springer)
- [109] Tsallis C and Bukman D J 1996 Anomalous diffusion in the presence of external forces: exact time-dependent solutions and their thermostatistical basis *Phys. Rev. E* **54** R2197
- [110] Tsallis C, Anteneodo C, Borland L and Osorio R 2003 Nonextensive statistical mechanics and economics *Physica A* **324** 89
- [111] Borland L and Bouchaud J-P 2004 A non-Gaussian option pricing model with skew *Quant. Finance* **4** 499
- [112] Caruso F, Pluchino A, Latora V, Vinciguerra S and Rapisarda A 2007 Analysis of self-organized criticality in the Olami–Feder–Christensen model and in real earthquakes *Phys. Rev. E* **75** 055101(R)
- [113] Rodríguez A, Schwämmler V and Tsallis C 2008 Strictly and asymptotically scale invariant probabilistic models of N correlated binary random variables having q -Gaussians as $N \rightarrow \infty$ limiting distributions *J. Stat. Mech.* P09006
- [114] Lagache T, Dauty E and Holcman D 2009 Quantitative analysis of virus and plasmid trafficking in cells *Phys. Rev. E* **79** 011921
- [115] Lagache T and Holcman D 2008 Quantifying intermittent transport in cell cytoplasm *Phys. Rev. E* **77** 030901
- [116] von Hippel P H and Berg O G 1989 *J. Biol. Chem.* **264** 675
- [117] Bauer M and Metzler R 2012 Generalized facilitated diffusion model for DNA-binding proteins with search and recognition states *Biophys. J.* **102** 2321
- [118] Sabri A, Xu X R, Krapf D and Weiss M 2020 Elucidating the origin of heterogeneous anomalous diffusion in the cytoplasm of mammalian cells *Phys. Rev. Lett.* **125** 058101
- [119] Janczura J, Balcerk M, Burnecki K, Sabri A, Weiss M and Krapf D 2021 Identifying heterogeneous diffusion states in the cytoplasm by a hidden Markov model *New J. Phys.* **23** 053018
- [120] He W, Song H, Su Y, Geng L, Ackerson B J, Peng H B and Tong P 2016 Dynamic heterogeneity and non-Gaussian statistics for acetylcholine receptors on live cell membrane *Nat. Commun.* **7** 11701
- [121] Díez Fernández A, Charchar P, Cherstvy A G, Metzler R and Finnis M W 2020 The diffusion of doxorubicin drug molecules in silica nanoslits is non-Gaussian, intermittent and anticorrelated *Phys. Chem. Chem. Phys.* **22** 27955
- [122] Yamamoto E, Akimoto T, Yasui M and Yasuoka K 2014 Origin of subdiffusion of water molecules on cell membrane surfaces *Sci. Rep.* **4** 4720
- [123] Tan P, Liang Y, Xu Q, Mamontov E, Li J, Xing X and Hong L 2018 Gradual crossover from subdiffusion to normal diffusion: a many-body effect in protein surface water *Phys. Rev. Lett.* **120** 248101
- [124] Beck C and Cohen E G D 2003 Superstatistics *Physica A* **322** 267
- [125] Beck C 2007 Statistics of three-dimensional Lagrangian turbulence *Phys. Rev. Lett.* **98** 064502
- [126] Luo L and Yi M 2019 Quenched trap model on the extreme landscape: the rise of subdiffusion and non-Gaussian diffusion *Phys. Rev. E* **100** 042136
- [127] Massignan P, Manzo C, Torreno-Pina J A, García-Parajo M F, Lewenstein M and Lapeyre G J Jr 2014 Nonergodic subdiffusion from Brownian motion in an inhomogeneous medium *Phys. Rev. Lett.* **112** 150603
- [128] Bouchaud J-P and Georges A 1990 Anomalous diffusion in disordered media: statistical mechanisms, models and physical applications *Phys. Rep.* **195** 127
- [129] Burov S and Barkai E 2020 Packets of spreading particles exhibit universal exponential tails *Phys. Rev. Lett.* **124** 060603
- [130] Chubynsky M V and Slater G W 2014 Diffusing diffusivity: a model for anomalous and anomalous yet Brownian diffusion *Phys. Rev. Lett.* **113** 098302
- [131] Jain R and Sebastian K L 2016 Diffusion in a crowded, rearranging environment *J. Phys. Chem. B* **120** 3988
- [132] Tyagi N and Cherayil B J 2017 Non-Gaussian Brownian diffusion in dynamically disordered thermal environments *J. Phys. Chem. B* **121** 7204
- [133] Chechkin A V, Seno F, Metzler R and Sokolov I M 2017 Brownian yet non-Gaussian diffusion: from superstatistics to subordination of diffusing diffusivities *Phys. Rev. X* **7** 021002
- [134] Cherstvy A G and Metzler R 2016 Anomalous diffusion in time-fluctuating non-stationary diffusivity landscapes *Phys. Chem. Chem. Phys.* **18** 23840
- [135] Sposini V, Chechkin A V, Seno F, Pagnini G and Metzler R 2018 Random diffusivity from stochastic equations: comparison of two models for Brownian yet non-Gaussian diffusion *New J. Phys.* **20** 043044
- [136] Yamamoto E, Akimoto T, Mitsutake A and Metzler R 2021 Universal relation between instantaneous diffusivity and radius of gyration of proteins in aqueous solution *Phys. Rev. Lett.* **126** 128101
- [137] Olivares-Rivas W, Colmenares P J and López F 2013 Direct evaluation of the position dependent diffusion coefficient and persistence time from the equilibrium density profile in anisotropic fluids *J. Chem. Phys.* **139** 074103
- [138] Hummer G 2005 Position-dependent diffusion coefficients and free energies from Bayesian analysis of equilibrium and replica molecular dynamics simulations *New J. Phys.* **7** 34
- [139] Li Y, Mei R, Xu Y, Kurths J, Duan J and Metzler R 2020 Particle dynamics and transport enhancement in a confined channel with position-dependent diffusivity *New J. Phys.* **22** 053016
- [140] English B P, Hauryliuk V, Sanamrad A, Tankov S, Dekker N H and Elf J 2011 *Proc. Natl Acad. Sci. USA* **108** E365
- [141] Cherstvy A G, Chechkin A V and Metzler R 2014 Particle invasion, survival, and non-ergodicity in 2D diffusion processes with space-dependent diffusivity *Soft Matter* **10** 1591
- [142] Cherstvy A G and Metzler R 2013 Population splitting, trapping, and non-ergodicity in heterogeneous diffusion processes *Phys. Chem. Chem. Phys.* **15** 20220
- [143] Leibovich N and Barkai E 2019 Infinite ergodic theory for heterogeneous diffusion processes *Phys. Rev. E* **99** 042138
- [144] Wang X, Deng W and Chen Y 2019 Ergodic properties of heterogeneous diffusion processes in a potential well *J. Chem. Phys.* **150** 164121
- [145] Fa K S and Lenzi E K 2005 Anomalous diffusion, solutions and first passage time: influence of diffusion coefficient *Phys. Rev. E* **71** 012101
- [146] Risken H 1989 *The Fokker–Planck Equation* (Heidelberg: Springer)
- [147] Lau A W C and Lubensky T C 2007 State-dependent diffusion: thermodynamics consistency and its path integral formulation *Phys. Rev. E* **76** 011123
- [148] Grebenkov D S, Sposini V, Metzler R, Oshanin G and Seno F 2021 Exact distributions of the maximum and range of random diffusivity processes *New J. Phys.* **23** 023014
- [149] Mattos T, Mejía-Monasterio C, Metzler R and Oshanin G 2012 First passages in bounded domains: when is the mean first passage time meaningful? *Phys. Rev. E* **86** 031143
- [150] Fiasconaro A and Spagnolo B 2011 Resonant activation in piecewise linear asymmetric potentials *Phys. Rev. E* **83** 041122

- [151] Fiasconaro A, Valenti D and Spagnolo B 2003 Role of the initial conditions on the enhancement of the escape time in static and fluctuating potentials *Physica A* **325** 136
- [152] Mantegna R N and Spagnolo B 1998 Probability distribution of the residence times in periodically fluctuating metastable systems *Int. J. Bifurcation Chaos* **08** 783
- [153] Guarcello C, Valenti D and Spagnolo B 2015 Phase dynamics in graphene-based Josephson junctions in the presence of thermal and correlated fluctuations *Phys. Rev. B* **92** 174519
- [154] Dubkov A A and Spagnolo B 2005 *Phys. Rev. E* **72** 041104
- [155] Giuffrida A, Valenti D, Ziino G, Spagnolo B and Panebianco A 2009 *Eur. Food Res. Technol.* **228** 767